

BRIGHT LESION DETECTION IN RETINAL IMAGES

ZHANG XIAOLI

A Thesis submitted for
the Degree of Master of Science

Department of Computer Science

School of Computing

National University of Singapore

· 2006 ·

Abstract

Digital retinal images are widely used as effective means of screening medical conditions such as diabetic retinopathy. The presence of bright lesions such as hard exudates and cotton wool spots is an indicator of diabetic retinopathy and automated detection of these bright lesions in retinal images is useful to reduce the cost of screening process.

This work is focused on automatic detection of two types of bright lesions, namely hard exudates and cotton wool spots in retinal images. Hard exudates appear as yellow-white small spots in retinal images. We developed a technique that utilize wavelet analysis to localize the hard exudates. Cotton wool spots are yellowish fluffy patches in retinal images. We used intensity difference map of contrast-enhanced retinal images to localize cotton wool spots. Then we validated the candidate cotton wool spots regions with two methods. The first method is eigenimages and the second method is Support Vector Machine(SVM) classification. We evaluated our algorithms with 1198 retinal images collected from local clinics. Our hard exudates detection algorithm achieved 97.9% sensitivity and 78.2% specificity. The SVM classification approach outperformed eigenimages and achieved 100% sensitivity and 82.8% specificity. With the high sensitivity and specificity, our proposed approach will be able to facilitate the automated screening in clinics.

Contents

Acknowledgments	1
1 Introduction	2
1.1 Motivation	2
1.2 Objective	5
1.3 Major Contribution of the Thesis	6
1.4 Organization	7
2 Literature Review	9
2.1 Lesion Detection	9
2.2 Hard Exudates Detection	11
2.3 Discussion	14
2.4 Wavelet Application in Medical Image Processing	15
3 Hard Exudates Detection	18
3.1 Wavelet Transform	18
3.2 Hard Exudates Detection	19
3.3 Experiment Results	25
4 Cotton Wool Spots Detection	29
4.1 Preprocessing	33

4.1.1	Image Normalization	33
4.1.2	Local Contrast Enhancement	37
4.2	Candidate Identification Step	40
4.3	Validation Step	46
4.3.1	Eigenimages	47
4.3.2	SVM Classification	50
4.4	Experiment	54
5	Conclusion and Future work	59
	Bibliography	66

List of Figures

1.1	Hard exudates in a retinal image	3
1.2	Cotton wool spots in retinal image	4
3.1	Wavelet decomposition and reconstruction	20
3.2	Lesions in retinal image	21
3.3	Summary of hard exudates detection using wavelet transform . . .	22
3.4	Detail images of wavelet decomposition	24
3.5	Magnitude computed from <i>HL</i> and <i>LH</i> components at level 1 and 2 .	25
3.6	Logical OR of resultant images of thresholding magnitude images . . .	25
3.7	Post-processing diagram	26
4.1	HL components at 4 levels wavelet decomposition of the image in Figure 1.2	30
4.2	Binary image resulting from thresholding HL component overlaid with the input image	31
4.3	Overview of cotton wool detection	32
4.4	Reference image	34
4.5	Histogram of reference image	35
4.6	Result of Histogram Specification	35
4.7	Histogram of RGB components	36

4.8	Histogram Equalization	38
4.9	Divide Image into 64x64 partially overlapping windows	39
4.10	Adaptive Histogram Equalization	41
4.11	Intermediate images	44
4.12	Lab Components of image in Fig 4.6	45
4.13	Segmentation Fuzzy C-mean clustering	46
4.14	Training images and average image	48
4.15	Smaller center window	53
4.16	Boundary of a window	54
4.17	False cotton wool spots detected by SVM classification	56

List of Tables

3.1	Coefficients of wavelet	22
3.2	Hard Exudates Detection	27
4.1	Comparison of the number of regions identified	55
4.2	Comparison of the number of images identified	57
4.3	SVM Classification Result	57
4.4	Experiment Results of the Two Approaches	57

Acknowledgments

First and most importantly, I am extremely grateful to my supervisor Dr. Lee Mong Li and Dr. Wynne Hsu. They have given me the most valuable guidance that an adviser can give her students. Their helpful comments, suggestions and insightful criticism are invaluable to my research work.

I am also very grateful to my labmates, Minghua, Li Ling, Xinyu and Gao Jiong for their continuous support and those valuable discussions and suggestions.

Finally, I would like to express my love and gratitude to my family who have always been supporting and encouraging me.

Chapter 1

Introduction

1.1 Motivation

Diabetic retinopathy is identified as a leading cause of blindness and visual impairment in many developed countries and accounts for 12,000 to 24,000 blind cases in United States alone every year [12]. Digital retinal images taken by special fundus camera are used for diabetic retinopathy screening. The presence of certain lesions in retina have proven to be a visible sign of diabetic retinopathy. Hard exudates and cotton wool spots are two types of bright lesions in retinal images that are considered indicative of the presence of diabetic retinopathy because they are the first retinal changes to develop in this disease. Hard exudates are yellow-white small spots, while cotton wool spots are white fluffy patches.

Figure 1.1 shows a retinal image that contains hard exudates. Hard exudates are visible as yellowish deposits in the retina. Their presence implies leaking retinal capillaries. The weakened capillary walls causes out-pouchings in their walls called microaneurysms, which may also leak. Exudates very frequently arrange themselves in a circular pattern in diabetes, and often a cluster of leaking microa-

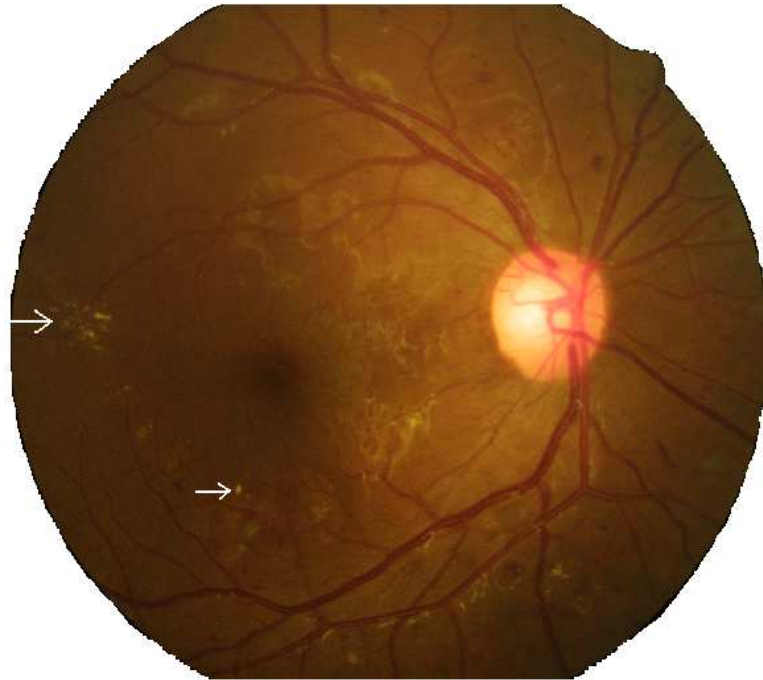


Figure 1.1: Hard exudates in a retinal image

neurysms appear in the middle of such a ring of exudates. This arrangement is called 'circinate exudates'. As with most other conditions, exudates affect vision only when they encroach on the macula, and hence the need for regular retinal screening of diabetic subjects so that any exudates approaching the macula may be treated. Automated detection of these lesions in retinal images produced from screening programmes will be useful to reduce the workload of the doctors reading the retinal images and facilitate the follow-up management of diabetic patients.

Figure 1.2 shows four cotton wool spots in a retinal image. Cotton wool spots are common features of diabetic retinopathy and appear as white fluffy opaque area in the sensory retina. They result from an arteriolar occlusion in the retinal nerve fibre layer. The evolution of cotton wool spots in diabetic retinopathy is somewhat variable. Many cotton wool spots associated with diabetic retinopathy persist for three or six months. As cotton wool spots resolve slowly, they often

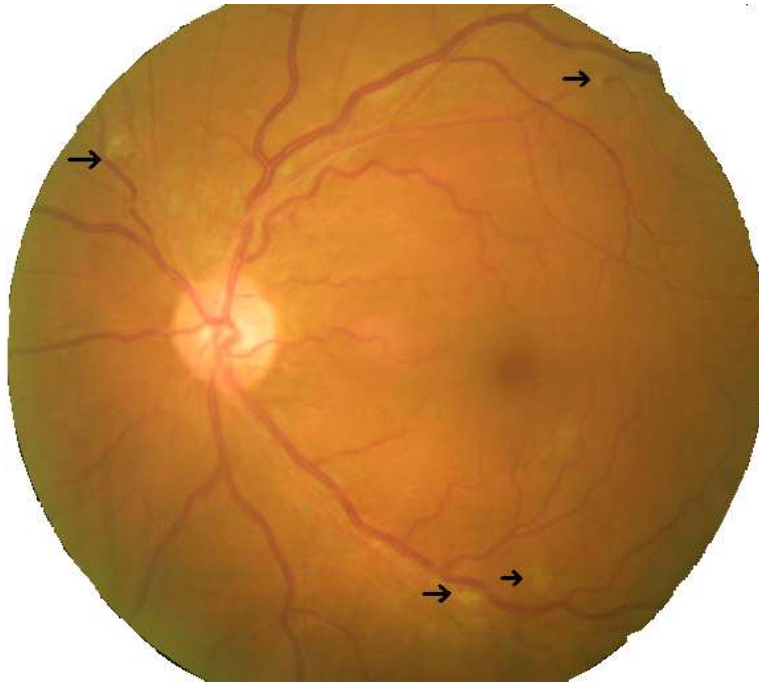


Figure 1.2: Cotton wool spots in retinal image

appear as multiple small round white dots. In diabetes cotton wool spots indicate advanced background or pre-proliferative stages of retinopathy. Cotton wool spots are usually related to Age-related Macular Degeneration in diabetes in radiation retinopathy transient and rarely remain visible for more than a few months. It is important to realize that cotton wool spots, exudates and retinal haemorrhages frequently co-exist since they may appear as a result of the same vascular disorders, the most common being diabetes and hypertension.

The detection of hard exudates and cotton wool spots in retinal images is a challenging task. The main obstacle is the extreme variability of the color of retinal images and the presence of retinal blood vessels. Different types of bright-colored lesions such as hard exudates, cotton wool spots and drusen may appear in one retinal image, which makes it difficult to detect hard exudates and cotton wool spots based on their intensity features. The algorithms proposed in [5,10,28]

to detect hard exudates are tested only on a small set of images. Zhang et al. [41] proposed an algorithm based on classification between cotton wool spots and other lesions and the achieved sensitivity is around 80% with 30 images. It is not very clear how their system will perform on large set of real-world images.

1.2 Objective

In this research, we are interested in developing sensitive and robust detection algorithms for hard exudate and cotton wool spots in digital retinal images which can be used for automated screening of diabetic retinopathy. We investigate how wavelet analysis can be utilized to localize hard exudates and cotton wool spots and techniques such as eigenimages and SVM classification, can be employed to detect cotton wool spots.

There has been a growing interest to use wavelets as a new transform technique for image processing. The aim of wavelet transform is to ‘express’ an input signal as a series of coefficients of specified energy. It has been used for the compression of medical images, CT(computerized tomography) reconstruction, wavelet denoising, feature extraction, image enhancement, etc. [16, 34] Given the intensity of hard exudates is relatively high compared to their background, we note that wavelet transform is suitable to detect them. We examine how wavelet transform can be used to detect the hard exudates, those bright spots where the sharp changes of intensity occur.

Eigenimage has been widely applied in face recognition [19,33], texture classification and retrieval [8]. Li et al. [21] used eigenimage for optic disc localization in retinal images. As cotton wool spots are relatively larger than hard exudates, they usually have high intensity in the center and have dim and fuzzy boundaries.

With these characteristics of cotton wool spots, we investigate how eigenimage can be used to detect cotton.

Support vector machine (SVM), is a type of learning machine based on statistical learning theory [31]. It has gained a lot of popularity in pattern classification of medical imaging due its satisfactory performance. Feature selection is quite crucial for classification problem. Since the cotton wool spots do not have uniform color, the color information of cotton wool spots is not sufficient to identify them. In this work, we explore other features of cotton wool spots, such as compactness, the number of pixels on the boundary, distance from centroid to the window center, etc.

1.3 Major Contribution of the Thesis

The thesis has contributed to the analysis of retinal images and the detection of bright lesions such as hard exudates and cotton wool spots in retinal images. The proposed wavelet-based detection algorithm provides an accurate method to detect hard exudates. To our best of our knowledge, this is the first work to utilize wavelet analysis to detect hard exudates. Our algorithm of detecting hard exudates using wavelet analysis has sensitivity of 97.9% and specificity of 78.2%. The wavelet approach captures the sharp color changes on the boundary of hard exudates and the good performance shows wavelet is suitable for hard exudate detection.

Cotton wool spots detection is a challenging task. Existing efforts are focused on detecting lesions and do not identify cotton wool spots directly. In this thesis, we described how eigenimages and SVM classification can be utilized to detect cotton wool spots. The proposed SVM classification approach is able to achieve

100% for Sensitivity and 82.8% for Specificity. The variation in color and shape of cotton wool spots make it very difficult to detect cotton wool spots. Our proposed approach reduces the variation in color in a pre-processing step and the candidate cotton wool spots are further validated using two different methods, eigenimages and SVM classification. The basic idea of Eigenimage approach is template matching. Since cotton wool spots do not have uniform shape, the Eigenimage approach does not perform as well as SVM classification approach.

We also demonstrate the robustness and reliability of our methods by evaluating them on a real world dataset of 1198 retina images which have been collected from local clinics. The experiment results indicate that the proposed approach have the potential to be applied to the real world.

1.4 Organization

The rest of the thesis is organized as follows.

Chapter 2 reviews the major in literature on lesion detection. Chapter 3 describes how the wavelet analysis is utilized for hard exudates detection and how domain knowledge of vessels is used to remove the false hard exudates. We also present the experiment results with 1198 images.

In Chapter 4, two different cotton wool spots detection approaches are discussed. The first approach is to use eigenimages. In this approach, an eigenimage is computed from training images and used to validate the candidate regions from thresholding intensity difference map. Secondly, the Support Vector Machine classification is employed to classify the candidate regions resulting from fuzzy c-mean clustering into true cotton wool spots and non-cotton wool spots. In order to give more insights into the three approaches, the results of these two

approaches are compared as well.

Chapter 2

Literature Review

There is an increasing interest for developing systems and algorithms that can help screen a large number of patients for sight threatening diseases like diabetic retinopathy with automated detection of these disease. Digital fundus images are used as tools to screen and diagnose diabetic retinopathy. Digital image processing is now being very practical and useful for diabetic retinopathy screening. Several examples of application of digital image processing techniques can be found in literature. In this chapter we present a survey on the major retinal image analysis systems and algorithms, which have been already proposed with the main highlight on hard exudates detection and cotton wool spots detection.

2.1 Lesion Detection

A number of systems ([5, 15, 36, 41]) have been developed to detect lesions in retinal images. The work in [36] dose not classify lesions into hard exudates, drusen or cotton wool spots, while others [5, 15, 41] developed systems to detect lesions and further differentiate them into different types of lesions.

Wang et al. [36] have implemented an algorithm to detect exudates in digital retinal images. Initially a non-linear brightness adjustment procedure is applied to retinal images in order to work with different illuminant conditions. Feature space is transformed in to spherical coordinates and feature space consisting intensity, theta and phi have been selected for further processing. Bayes rule is next employed to derive an appropriate discriminant function for the algorithm. Selected lesion regions are next verified by adaptive thresholding. The enhanced algorithm has been tested against 100 digital retinal images and achieved 100% sensitivity and 78% specificity in detecting exudates.

Ege et al. [5] developed a screening system for diabetic retinopathy. The background of a retinal image was estimated using a 31x31 median filter on the original raw image. A threshold above the estimated background was selected to extract the bright objects and a threshold below the estimated background was chosen to extract the dark objects. Abnormal appearances (cotton wool spots, exudates, haemorrhages and microaneurysms) were distinguished by extracting features and feeding the features into a statistical classifier for pattern recognition. They also implemented a shape estimation routine using region growing in order to get the features on shapes. The classification was done based on features such as color, size, shape etc. The efficiency of three statistical classifiers, Bayesian, Mahalanobis, and KNN(k-nearest neighbor) classifier were discussed. The Mahalanobis classifier has given the best results; microaneurysms, hemorrhages, exudates, and cotton wool spots were detected with a sensitivity of 69%, 83%, 99%, and 80% respectively.

Katz et al. [15] and Goldbaum et. al. [10] have attempted to discriminate colored objects such as exudates, cotton wool spots and drusen in the scanned retinal images using a Mahalanobis classifier. Initially the algorithm converts the

color space to spherical coordinates and use the theta and phi for processing. To quantify the separability of three classes, Mahalanobis classifier and the jackknife technique have been used. Performance studies with 30 scanned retinal images have given 70% sensitivity for exudates, 70% sensitivity for cotton wool spots and 50% sensitivity for drusen.

Zhang et al. [41] applied Fuzzy C-Means clustering in Luv color space to the whole image and this resulted in a large number of segmented areas. They used two-step classification to classify these segmented areas into hard exudates and cotton wool spots. In fact, many of these areas were non-lesion related. As a result, the accuracy of classification was affected by these non-lesion related areas. Hence, to overcome this, in our research, we will use intensity difference map to identify potential cotton wool spots and Fuzzy C-Means clustering to refine the segmentation before classification.

2.2 Hard Exudates Detection

Previous hard exudates detection algorithms are mainly based on color information, shape, texture features, etc. They can be divided into four main categories, thresholding [24, 27, 28, 37], region growing [21], clustering [14], classification [9, 25], and a combination of above techniques [29].

Ward et al. [37] have implemented shade correction routine to reduce the shade variations in the fundus image. The background was considered sufficiently uniform, and the hard exudates were detected by grey-level thresholding.

Phillips et al. [27, 28] have proposed an adaptive thresholding technique for automated detection and quantification of retinal exudates. In the pre-processing stage, the image features were sharpen by convolution with a shade correction

kernel and median filtering to generate a smoothed image. It required the user to select the region of interest and sub-images of predefined size were created from the region of interest. The threshold was set with consideration of the characteristics of each image. The algorithm was evaluated on 14 scanned retinal images and it reported 87% mean sensitivity and 85% mean specificity.

Liu et al. [24] proposed another dynamic thresholding based method to detect exudates. A retinal image was firstly divided into subimages consisting 64x64 pixels with 50% overlap with each other. A dynamic threshold was selected based on the histogram of subimages. Those subimages which have uni-modal histogram were considered as the retinal background. After that, thresholding is applied to those subimages with bi-modal distribution or wide spread distribution. All the pixels whose intensity values were above the threshold were classified as exudates pixels. Region growing was employed to cluster these pixels together. They carried out experiment on 20 fundus images, out of which 7 images contain hard exudates. Their system failed to detect hard exudates in 2 images.

Li et al. [22] presented a combined method of edge detection and region growing to detect hard exudates. Luv color space was chosen as the suitable color space for exudates detection. A retinal image is divided into 64 subimages. Seeds in a subimage are selected and the region was allowed to grow from the seed until reaching an edge or large gradient. The edges were detected by Canny edge detector and the thresholds of edge detector were determined based on a fixed percentile of total number of pixels. If any hard exudate was detected in a subimage, the presence of hard exudates was identified. They reported 100% sensitivity and 71% specificity on 35 tested images.

Hsu et al. [14] propose an algorithm to improve the reliability of exudates detection by using domain knowledge. The cluster of lesions were found first by

dynamic clustering algorithm. Following that, hard exudates were differentiated from other lesions (drusen, cotton wool spots, etc.) with domain knowledge of these other lesions. Domain knowledge of location of vessels were used to remove those high intensity artifacts near large retinal vessels as results of light reflection. They reported 100% sensitivity and 74% specificity on 384 tested images.

Gardner et al. [9] have presented a neural network based system to detect various diabetic retinopathy lesions in digital retinal images. An artificial neural network has been trained with back-propagation algorithm to recognize features in 179 retinal images (147 diabetic and 32 normal). The effects of digital filtering techniques and different network variables have been assessed at the training stage. 200 diabetic and 101 normal images were then randomized and used to evaluate the networks performance against an ophthalmologist. Detection rates were 91.7%, 93.1% and 73.8% for recognition of vessels, exudates, and hemorrhages respectively. It has achieved sensitivity of 88.4% and a specificity of 83.5% for the detection of diabetic retinopathy.

Osareh et al. [25] first normalized the retinal images by using histogram specification such that their frequency histograms matched a selected reference image distribution. Then they applied an image segmentation approach based on a coarse and fine stages. The segmentation on coarse stage produced an initial classification into a number of classes and the center for each class. In the fine stage, Fuzzy C-mean (FCM) clustering assigned any remaining un-classified pixels to the closest class based on the minimization of an objective function. In the following step, they used neural network to classify the segmented region into exudate or non-exudates. Their evaluation of their system on 67 retinal images were able to achieve 95.0% sensitivity and 88.9% specificity.

Sinthanayothin et al. [29] developed a system to detect diabetic retinopathy

automatically. Their system pre-processes the retinal images to enhance their contrast by using locally adaptive approach. Their identification of candidate bright lesions(hard exudates) was done by recursive region growing and adaptive intensity thresholding and the dark lesions(haemorrhages and microaneurysms) are identified in a similar way but with the additional use of an edge enhancement operator, called a ‘moat operator’. They then classify them into true hard exudates or noise by artificial neural network. The features they used are the size, shape, hue and intensity of each candidate. Their evaluation of the system was done on 30 images. From the 30 images, 60780 candidate hard exudates were identified. Their classification achieved 88.5% sensitivity and 99.7% specificity. However, their measurements were based on 10x10 pixel grids which were identified by the ophthalmologist as exudate or non-exudate regions.

2.3 Discussion

To summarize, the research done on lesion detection in retinal images involves five main techniques, namely, thresholding [5, 24, 27, 28, 36, 37], region growing [21], clustering [14], classification [9, 10, 15, 25], and a combination of above techniques [29, 41].

The approaches proposed in [18, 20, 27, 28, 37] used thresholding techniques based on the intensity histogram. Simple thresholding techniques are highly undesirable for lesion detection, as the variation in the background intensities makes it difficult to find a proper threshold. Although adaptive techniques tend to give much better results, it is difficult to test its robustness and it is not sufficient to distinguish among different types of bright lesions including hard exudates and cotton wool spots. The results of these approaches depend on the

quality of the images.

Region growing techniques work well on the basis of suitable seeds selection. The criteria of region growing is usually defined on the relations between the intensities of the neighboring pixels. Even given the seeds are well selected, the criteria of region growing is hard to define due to inhomogeneous illumination of background and uneven intensity of lesions.

On the other hand, statistical classifiers based techniques and neural networks makes lesion detection more robust. [5, 10, 15] employed classification techniques to detect hard exudates. Their results are highly dependent on the training images. The other lesions that have similar shape and color features are difficult to differentiate using the classifier. Statistical classifiers such as Mahalanobis classifier [5, 10, 15] and Bayes classifier [5, 36] were reported with good result in detecting lesions. Clustering algorithms has been employed to achieve initial segmentation of bright lesions. [25] claimed that Support Vector Machine has advantages compared to Neural networks based systems as they can achieve a trade-off between false positive and false negatives. The performance of classification techniques depends on proper selection of the features.

2.4 Wavelet Application in Medical Image Processing

The advancement in wavelet theory has sparked researchers' interest in the application of wavelet in medical image processing [16, 34]. Here we summarized three of the applications.

Wavelet applications in medical imaging have been mainly on image compression, image denoising, texture features extraction, etc. In our work, we explored

wavelet application in localizing hard exudates in retinal images.

1. Noise Reduction

Wavelet application in noise reduction is not specific to medical imaging. The approach proposed by Weaver et al. [38] was to compute an orthogonal wavelet decomposition of the image and apply soft thresholding rule on the coefficients. Noise reduction is usually used in the pre-processing stage followed by image enhancement in image processing.

2. Image Enhancement

The objective here is to accentuate the image features that are related to clinical diagnosis but are difficult to view in normal conditions. For example, the contrast between soft tissues of the breast is small in mammography and a relatively minor change in mammary structure can signify the presence of a malignant breast tumor. Laine et al. [17] proposed wavelet-based contrast enhancement method for mammographic screening purpose.

3. Detection of Microcalcifications in Mammograms

The presence of clusters of fine, granular microcalcifications is one of the primary warning signs of breast cancer. Microcalcification have high attenuation, a good visibility property but their sizes are usually very small, which makes them extremely difficult to view. Strickland [32] proposed a wavelet-base method to detect the microcalcifications by thresholding in wavelet domain. They used wavelet transform to detect the microcalcification in mammograms. In their work, they apply B-spline wavelet transform to the mammograms, threshold the wavelet components at 6 levels, combine the binary results, and finally, carry out an inverse wavelet transform.

To date, no work has been done to apply wavelet for the detection of hard exudates. In the next chapter, we will describe how wavelet can be utilized to detect hard exudates in retinal images.

Chapter 3

Hard Exudates Detection

Hard exudates appear as small yellow-white spots in retinal images. They have relatively distinctive boundaries. The aim of wavelet transform is to ‘express’ an input signal as a series of coefficients of specified energy. Wavelet transform can capture the sharpen changes in the images, thus the distinctive boundaries of hard exudates are captured in the components from wavelet transform.

In this chapter, we present an approach to detect hard exudates using wavelet analysis.

3.1 Wavelet Transform

Wavelet transform has become a popular technique for image analysis and compression. In the 2-D wavelet decomposition, the low-pass filter L , and high-pass filter H are applied to the image in both horizontal and vertical directions. These filters produce three highpass subbands HL , LH and HH (also called detail coefficients), and one lowpass subband LL (also called approximation coefficients) [3]. The LL component can be further decomposed by repeating the same pro-

cess.

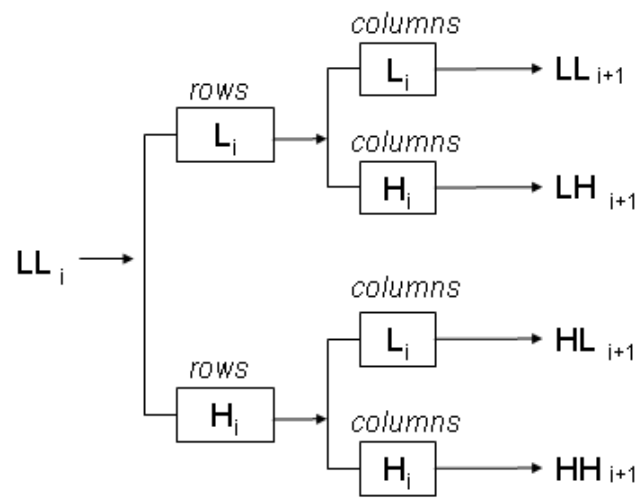
With discrete wavelet transform, the HL , LH , HH and LL components are down-sampled and their size is half of the input signals. The multi-level decomposition produces HL , LH and HH components at different scales, and the multi-resolution analysis can be done on these components. Hence, if we decompose an image of size $M \times N$ at level i , the sizes of the resulting detail images are $(M/2^i) \times (N/2^i)$.

On the other hand, in stationary wavelet transform, the image is not down-sampled but the filter is up-sampled. With this multi-resolution decomposition, we can analyze the image in different scales.

The algorithm of two-dimensional stationary wavelet decomposition is illustrated in Figure 3.1(a), where LH_{i+1} , HL_{i+1} and HH_{i+1} correspond to different frequency sub-bands at resolution level $i + 1$. LH_i is computed by filtering the rows with low-pass filter L followed by filtering the columns with high-pass filter H . Since the high-pass filter is applied to the columns of the input image, the component LH_i captures the vertical energy changes. Similarly, HL_i contains the horizontal features and HH_i corresponds to the diagonal features. The wavelet reconstruction(Figure 3.1(b)) is basically the reverse of wavelet decomposition. Following column convolution, the corresponding images are summed. The final image is the summation of the two images resulting from row convolutions.

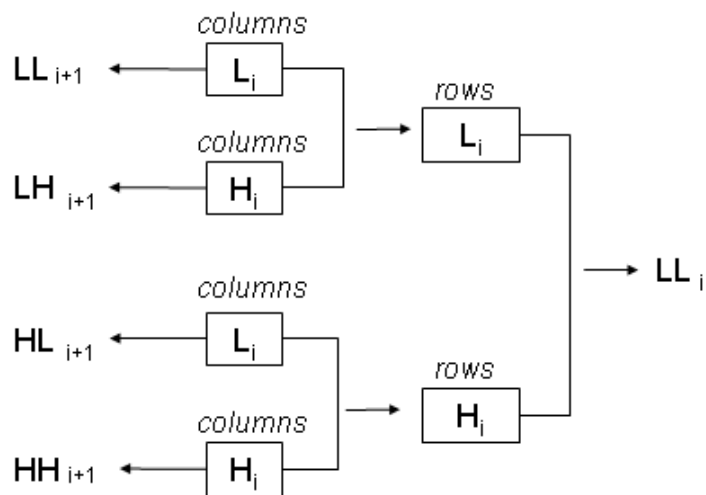
3.2 Hard Exudates Detection

The intensity of hard exudates is relatively high compared to their background. These characteristics make them suitable to be detected by wavelet transform, as wavelet transform can detect those spots where the sharp changes of intensity



Where $\begin{matrix} \text{rows} \\ \boxed{X} \end{matrix}$ convolves with filter X the rows of entry
 Where $\begin{matrix} \text{columns} \\ \boxed{X} \end{matrix}$ convolves with filter X the columns of entry

(a) Deomposition



Where $\begin{matrix} \text{rows} \\ \boxed{X} \end{matrix}$ convolves with filter X the rows of entry
 Where $\begin{matrix} \text{columns} \\ \boxed{X} \end{matrix}$ convolves with filter X the columns of entry

(b) Reconstruction

Figure 3.1: Wavelet decomposition and reconstruction

occur.

In Figure 3.2, the hard exudates are marked out by black circles and the green circle marks out the other type of lesion, cotton wool spots. Both of them are relatively bright compared to the background, and it is difficult to differentiate them based on the intensity values. However, the hard exudates have stronger features in the wavelet domain, as the intensity changes in cotton wool spots are gradual. Liu et al. [24] has shown that hard exudates have higher intensity level

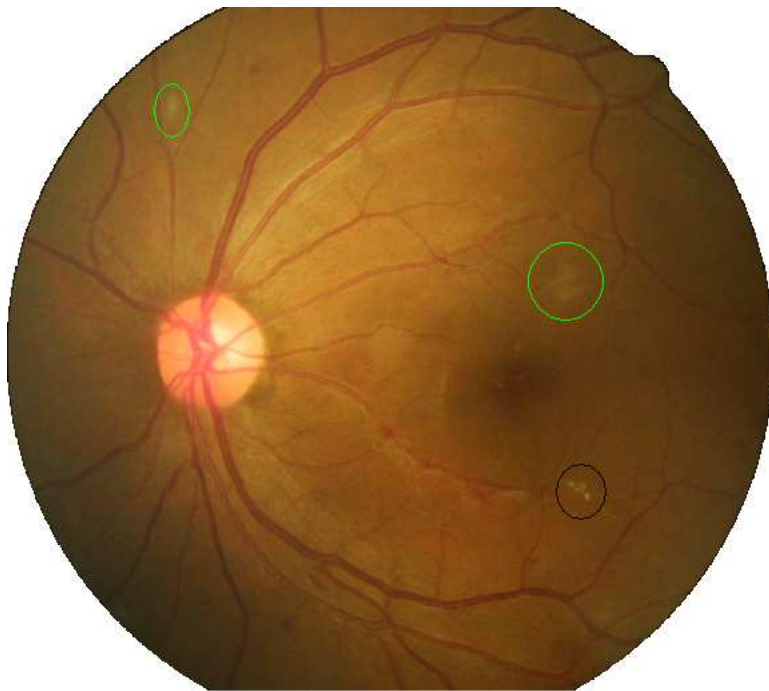


Figure 3.2: Lesions in retinal image

compared to background in the green layer than than other two layers.

In this section, we present the proposed method of wavelet-based exudate detection. In order to remove the artifacts due to light reflectance along the vessel, we also implement a routine to remove these artifacts. The whole process is summarized in Figure 3.3. We first smooth the image using 3x3 mean filters. As explained in Section 3.1, the HL , LH and HH components of wavelet decom-

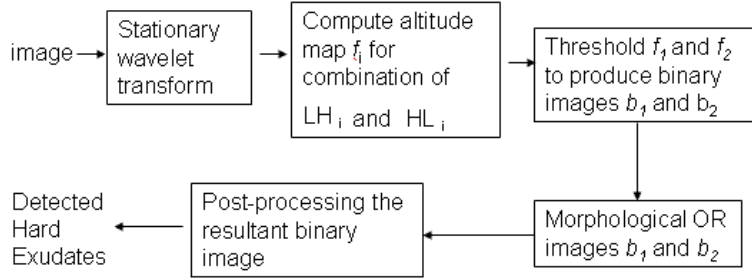


Figure 3.3: Summary of hard exudates detection using wavelet transform

position are sensitive to horizontal, vertical, and diagonal features respectively, the small bright hard exudates usually correspond to large coefficients in these 3 components.

To detect hard exudates in retinal images, we will use the absolute values of these components, as the large absolute values correspond to sharp intensity changes of the image and the sign of these components corresponds to the direction of the intensity changes, which is not of our concern.

n	l	h
1	0.0352	-0.3327
2	-0.0854	0.8069
3	-0.1350	-0.4599
4	0.4599	-0.1350
5	0.8069	0.0854
6	0.3327	0.0352

Table 3.1: Coefficients of wavelet

The detection of hard exudates utilizes the HL and LH components, as the features that appear in HH component are in diagonal orientation and they appears in HL and LH components as well. The wavelet we chose is Daubechies wavelet whose filter length is 6. Its coefficients are shown in Table 3.1.

The input image is decomposed at resolution level 2. At each level, the filter is upsampled in order to have decomposition at different scales. At level 3, the

length of filter will be too large for the hard exudates. Figure 3.4 shows the 6 detail images(Figure 3.4(b) (g)) of input image(Figure 3.4(a)) after the wavelet decomposition.

For each level i , from HL_i and LH_i components, we compute the magnitude as follows:

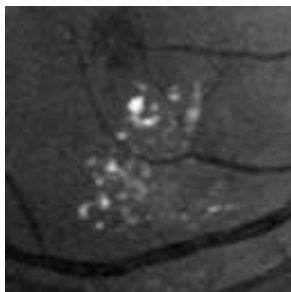
Let $h_i(x, y)$ be the value of HL_i at the pixel (x, y) and $g_i(x, y)$ be the value of LH_i at pixel (x, y) , then the magnitude at the pixel (x, y) is

$$f_i(x, y) = \sqrt{h_i^2(x, y) + g_i^2(x, y)}.$$

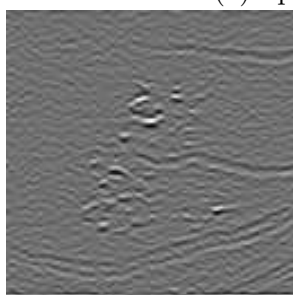
A non-horizontal feature corresponds to smaller coefficients in HL components than a horizontal feature, but it corresponds to larger coefficients in LH components. The magnitude, which is $\sqrt{HL^2 + LH^2}$, represents the energy level of a feature, regardless of its direction.

f_1 and f_2 are shown in Figure 3.5. Thresholding f_1 and f_2 produces two binary images. By applying the logical OR operation to the two binary images, we extract those spots where the sharp changes happen into a single binary image. The threshold is chosen based on a fixed percentile of the histogram of f_i . The binary image produced by logical OR is shown in Figure 3.6 and its original image is shown in Figure 3.4(a).

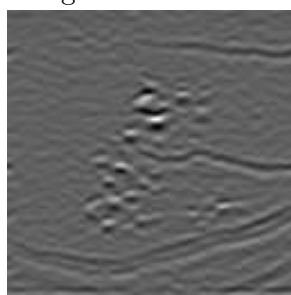
The small noises can simply be removed by morphology open operation with disk structure. The high intensity artifacts near the large vessels as a result of light reflection are also detected in the binary image. Such artifacts are removed by removing all the areas connected to the vessels detected by [6]. A few steps are needed to remove these artifacts along the vessel. Firstly, morphology open, close and dilation were applied the vessel image to close up the broken vessels and dilate the vessel to cover the reflection along the vessels. After that, region growing technique was applied, using the binary image produced by morphological OR



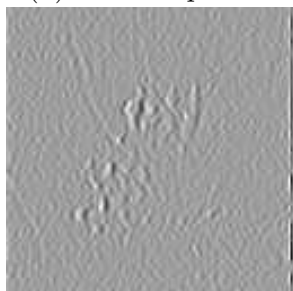
(a) Input Image



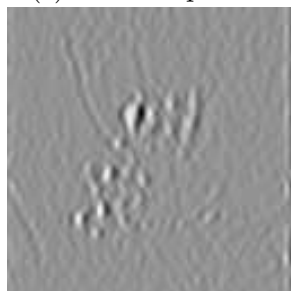
(b) HL_1 component



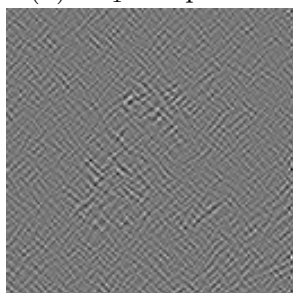
(c) HL_2 component



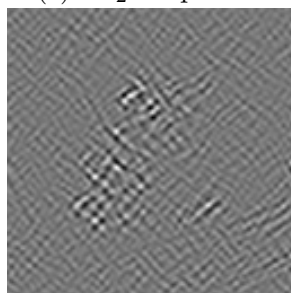
(d) LH_1 component



(e) LH_2 component



(f) HH_1 component



(g) HH_2 component

Figure 3.4: Detail images of wavelet decomposition

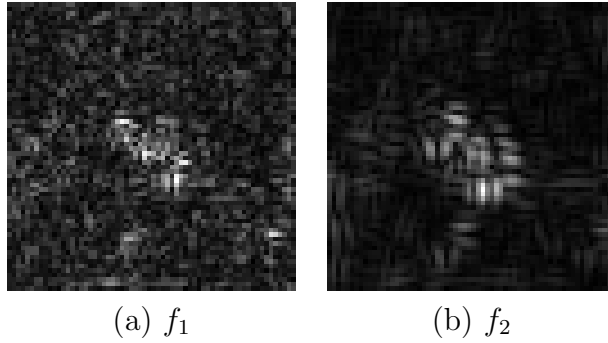


Figure 3.5: Magnitude computed from HL and LH components at level 1 and 2

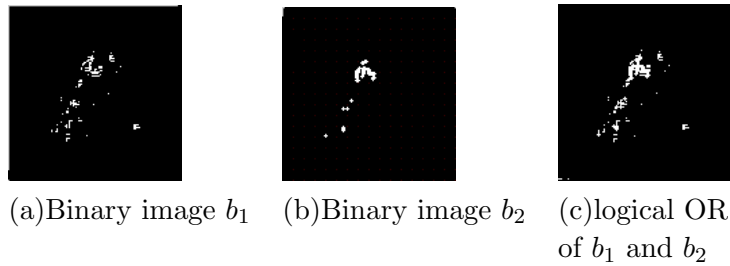


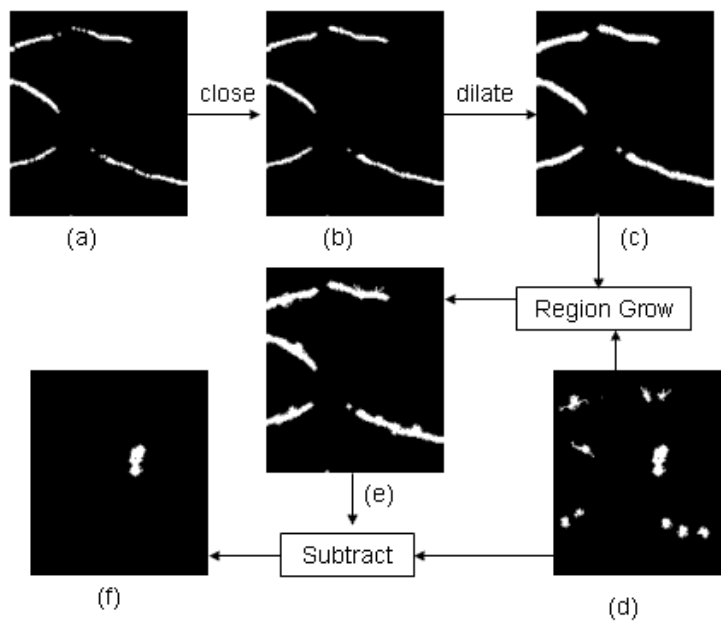
Figure 3.6: Logical OR of resultant images of thresholding magnitude images

operation as a mask image, to remove any detected area that was connected to any vessels.

To summarize, two levels wavelet decomposition are performed and the hard exudates are identified based on the combination of 4 of the resulting components. To remove the reflection along the vessels, the domain knowledge of vessels are taken into consideration.

3.3 Experiment Results

We evaluate our hard exudate detection approach with a large realworld dataset of 1198 consecutive images. Out of those 48 of which contain hard exudates. These images contain artifacts and retinal lesions and the quality of these images varies from poor to good. We compared the results of our hard exudates detection



- (a) vessel image,
 (b) morphological closing of (a),
 (c) morphological opening of (b),
 (d) binary image from wavelet analysis,
 (e) growing vessels in (c) based on (d),
 (f) subtract (e) from (d)

Figure 3.7: Post-processing diagram

algorithm with those given by the two retinal specialists.

We also compare our results with the algorithm proposed by Hsu et al. [14]. Their algorithm first find the cluster of lesions, including drusen, cotton wool spots and hard exudates, by dynamic clustering. Then the hard exudates are differentiated from other lesions based on the color differences between lesions and background.

We use two measurements, Sensitivity and Specificity, to evaluate the performance. Sensitivity is defined as the ratio of number of images where the hard exudates are localized correctly to the total number of images where the hard exudates are identified by the retinal specialist in the image. Specificity is the ratio of number of images where no hard exudates are detected to the total number of images where no hard exudates are identified by the retinal specialist.

Table 3.2 shows our experiment results. Our system can correctly localize the hard exudates in 47 images from 48 images that contains hard exudates. Our system gives false positive tests for the 251 images out of 1150 images that do not contain any hard exudates. Hence, we can achieve $(1150 - 251)/1150 = 78.2\%$ specificity. The result are compared to two retinal specialists' diagnosis in Table 3.2. Moreover, we also evaluated the algorithm proposed by Hsu. et al. [14] with these 1198 images and compared their results in Table 3.2) with ours.

	Doctor 1	Doctor 2	Algorithm in [14]	our result
Sensitivity	91.7%	93.75%	84%	97.9%
Specificity	91.9%	95.5%	80%	78.2%

Table 3.2: Hard Exudates Detection

Our experiment results with 1198 images show that our system are more robust than the system proposed by Hsu et al. [14]. In their algorithm, the hard exudates are differentiated from other lesions such as drusen and cotton

wool spots by clustering them in 3-D spherical coordinates. It achieved 100% sensitivity for the tested 543 images. However, it is not robust enough to handle more images, as the 3-D spherical coordinates are not sufficient to differentiate hard exudates from other lesions and noises. Our approach is to detect hard exudates in wavelet domain at multi-resolutions. The features of hard exudates are well represented in wavelet domain, which makes the detection easier.

Chapter 4

Cotton Wool Spots Detection

Cotton wool spots appear as yellow-white fluffy opaque area (Figure 1.2) in the retinal images. Similar to hard exudates detection, one obstacle of the detection of cotton wool spots has been that the reflectance of the normal background, on which the pathology is superimposed, is inherently non-uniform. Given two cotton wool spots, one near the optic disc and one further away, the observer will see them differently in the retinal image. The one near the optic disc will appear brighter. Moreover, cotton wool spots are more difficult to detect than hard exudates, as they have irregular shapes and their sizes vary greatly.

We investigate the application of wavelet analysis in localizing cotton wool spots. While the hard exudates have high coefficients in wavelet images of level 1 and level 2, cotton wool spots do not become visible until level 3 and level 4. In Figure 4.1, the HL components at 4 levels of wavelet decomposition are shown. The original input image (Figure 1.2) contains four cotton wool spots. We can see that the cotton wool spots are more obvious in level-4 images.

To identify candidates of cotton wool spots, we threshold the level-4 HL and LH components based on a fixed percentile. An example of the binary image

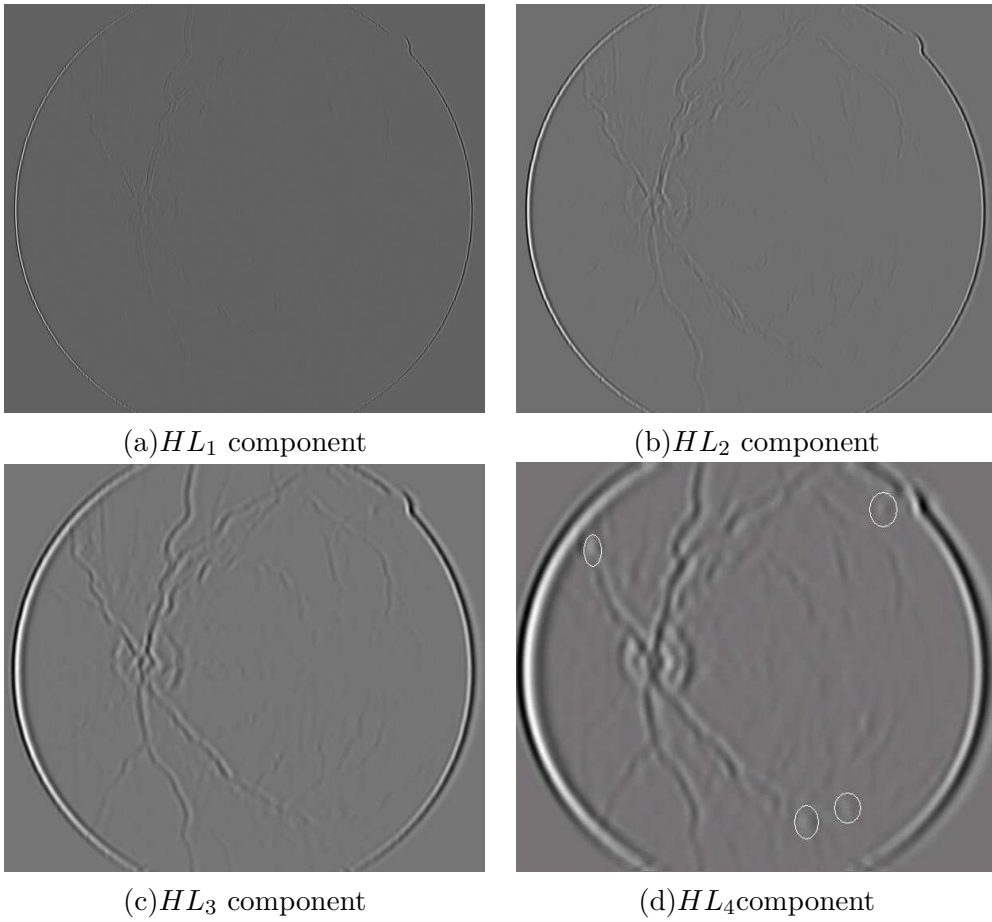


Figure 4.1: HL components at 4 levels wavelet decomposition of the image in Figure 1.2

produced by thresholding HL components at level 4 (overlaid on the original image) are shown in Figure 4.2, in which all the four true cotton wool spots are identified. Our experiment on 1198 retinal images shows that during the

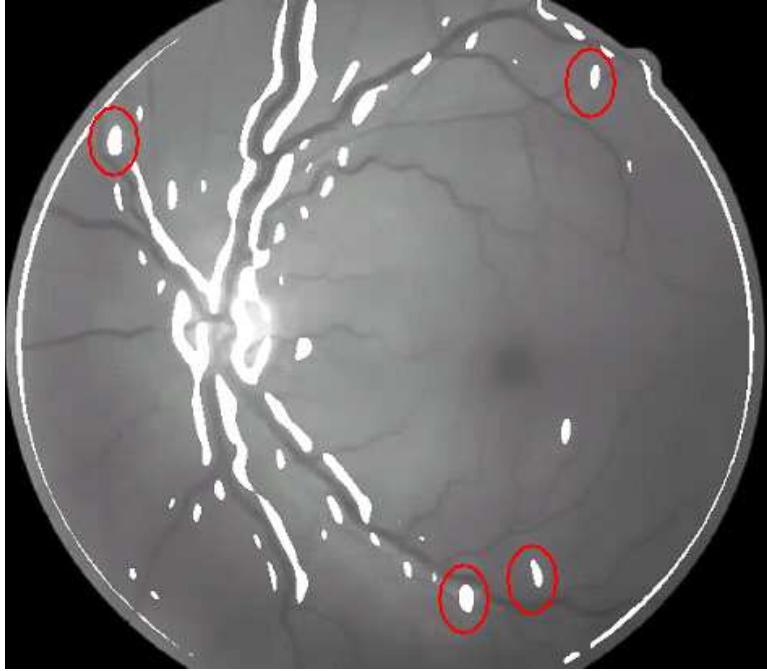


Figure 4.2: Binary image resulting from thresholding HL component overlaid with the input image

candidate identification step, all the true cotton wool spots are indeed selected as candidate patches. However, the step has also resulted in a large number of false candidate patches being highlighted. These false candidate patches are the reflection along vessels, artifacts, and other noises. The large number of candidate patches makes it difficult to validate the true cotton wool spots. Moreover, when the cotton wool spots are near retinal vessels, they are identified as part of the patches that correspond to the reflection along the vessels.

With these problem, we developed a strategy to detect cotton wool spots in two steps: a candidate identification step and a validation step. The candidate

identification step identifies potential regions that may contain cotton wool spots. The validation step checks whether the regions identified truly contain cotton wool spots. Two different approaches are presented for the validation step and their experiment results are compared.

In order to remove the non-uniform illuminant conditions among different retinal images, the retinal images are first normalized by using histogram specification. To deal with the variation of intensity in a retinal image, the local contrast of each image is enhanced using adaptive histogram equalization technique. After the color normalization and local contrast enhancement, the suspected regions are first localized based on the difference map of intensity. The Fuzzy-C means clustering is employed to refine the segmentation of the bright regions. The segmented bright regions are further classified into cotton wool spots and non-cotton wool spots by using two different approaches, eigenimages and Support Vector Machine Classifier. Figure 4.3 shows the overview of our cotton wool detection process.

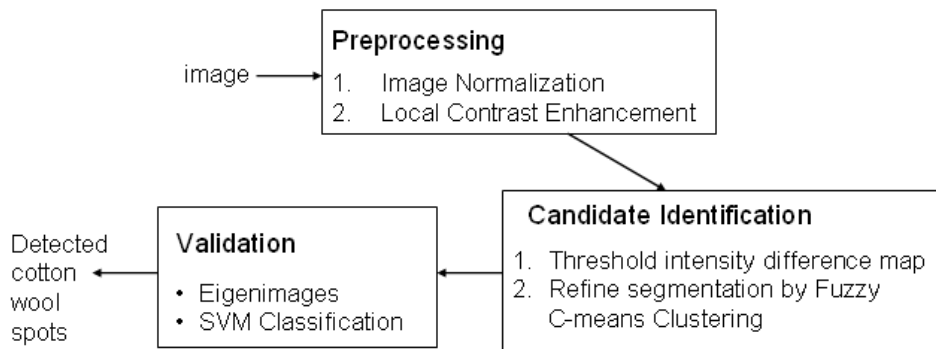


Figure 4.3: Overview of cotton wool detection

4.1 Preprocessing

4.1.1 Image Normalization

As the retinal images were taken by different user at different hospitals, the illumination of retinal images are different. Due to the wide variations in the color of retinal images from different patients, the bright lesions in some region of one image may appear dimmer than the background color of other regions in other images. The variation in color makes it difficult to detect lesions based on their color information. To reduce the variation, the color of the set of images are normalized before further processing. In order to improve the overall performance, normalization of the illumination of different images is necessary.

Histogram specification [11] is employed to perform color normalization. This modifies a color value in the given original image so that the resultant intensity distribution matches a desired distribution. Let $p_r(t)$ and $p_z(w)$ represent the probability density distribution functions of the values of one color channel of the original and desired image, respectively. The cumulative density distribution of the original image is denoted as $T(r)$, then $T(r)$ is computed as follows:

$$T(r) = \int_0^r p_r(t)dt$$

The cumulative density distribution of the desired image is denoted as $G(z)$, then $G(z)$ is computed as follows:

$$G(z) = \int_0^z p_z(w)dw$$

$T(r)$ and $G(r)$ should be identical density distribution. Thus $T(r) = G(z)$. Therefore, z must satisfy the condition $z = G^{-1}[T(r)]$. Thus, all r values in

original image is mapped to z values for the desired image.

Since retinal images are color images, this process is applied to each color channel of RGB channels independently. A well-illuminated reference image (Figure 4.4) is selected and its histogram (Figure 4.5) is used as a reference. All other retina images are transformed so that their histogram matched the reference histogram. Compared to histogram equalization, using which we can only generate one type of output image with uniform histogram, histogram specification can generate an output image with any specified histogram.

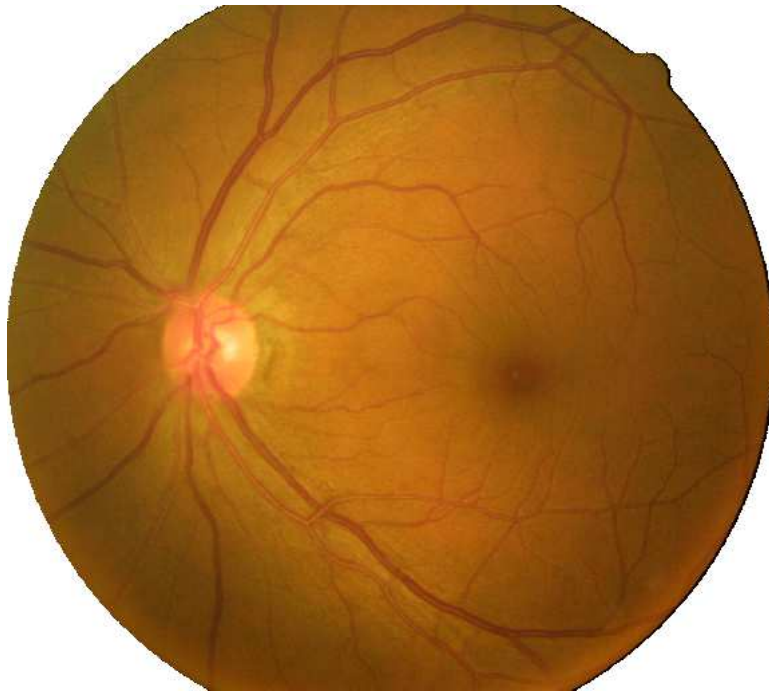


Figure 4.4: Reference image

To demonstrate the color normalization effect, a different color retinal image and its normalized version are shown in Figure 4.6(a) and (b). The histograms of RGB channel before and after histogram specification can be seen in Figure 4.7(a),(b) and (c). The normalization process modifies the color distributions of the considered image to match the reference image's distribution. This can

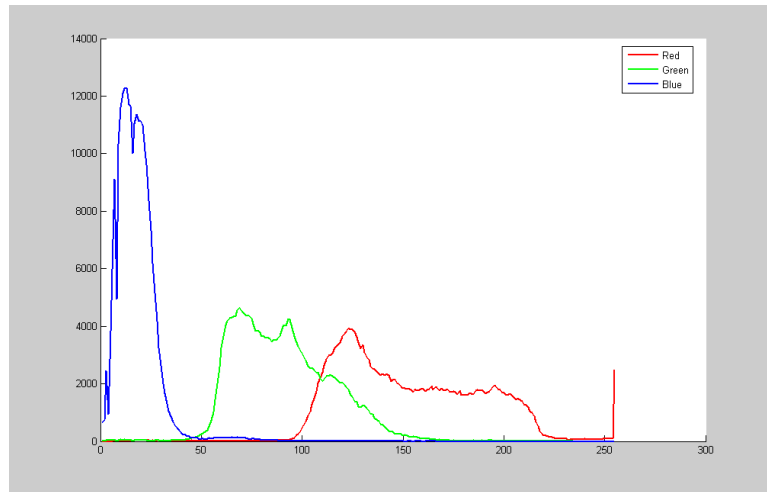
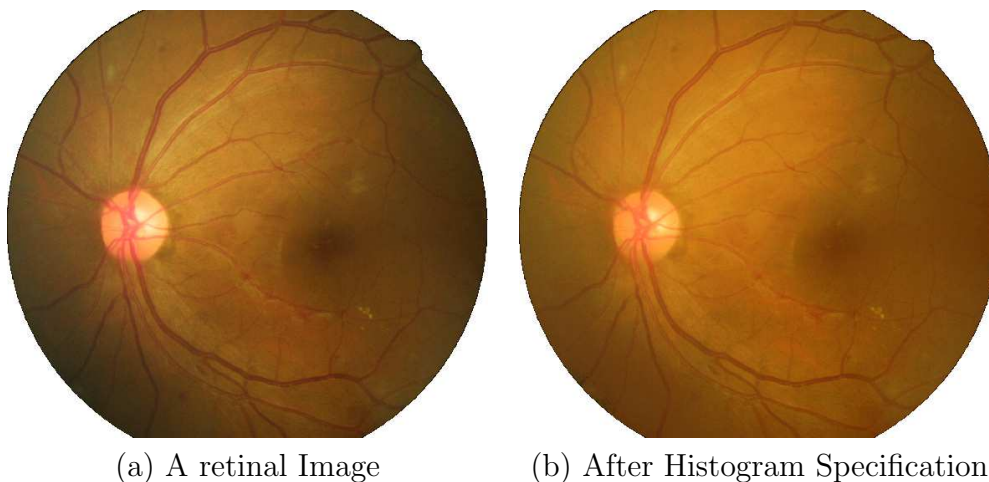


Figure 4.5: Histogram of reference image

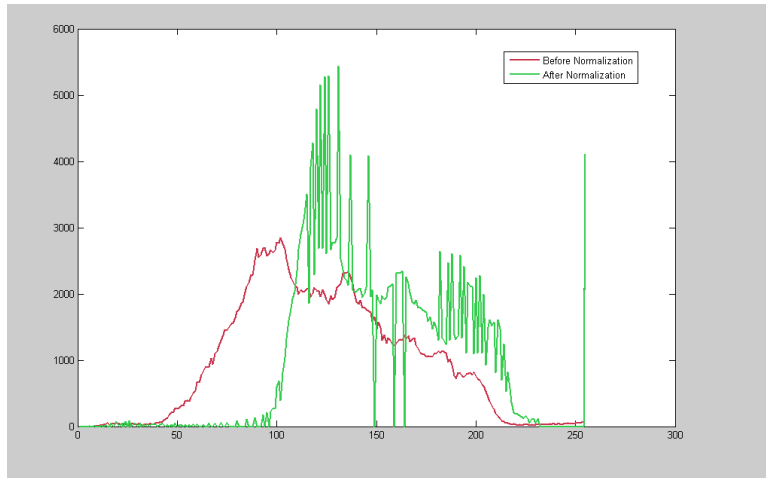
clearly be seen from comparison of the normalized image histograms (Green lines in in Figure 4.7) with the reference image’s histograms(in Figure 4.5). The color normalization process improves the clustering ability of the different lesion types and removes the variation due to the retinal pigmentation differences between individuals.



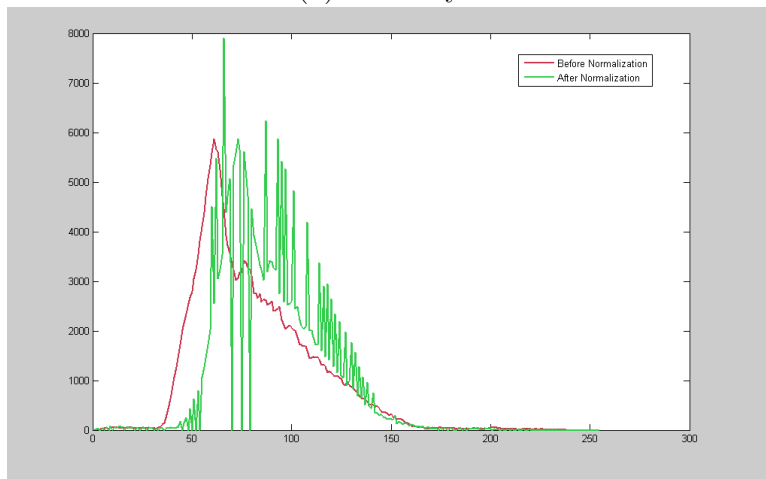
(a) A retinal Image

(b) After Histogram Specification

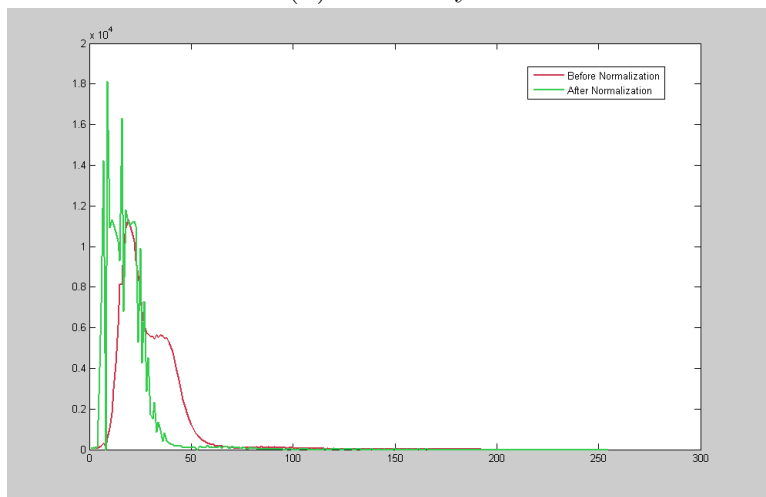
Figure 4.6: Result of Histogram Specification



(a) Red Layer



(b) Green Layer



(c) Blue Layer

Figure 4.7: Histogram of RGB components

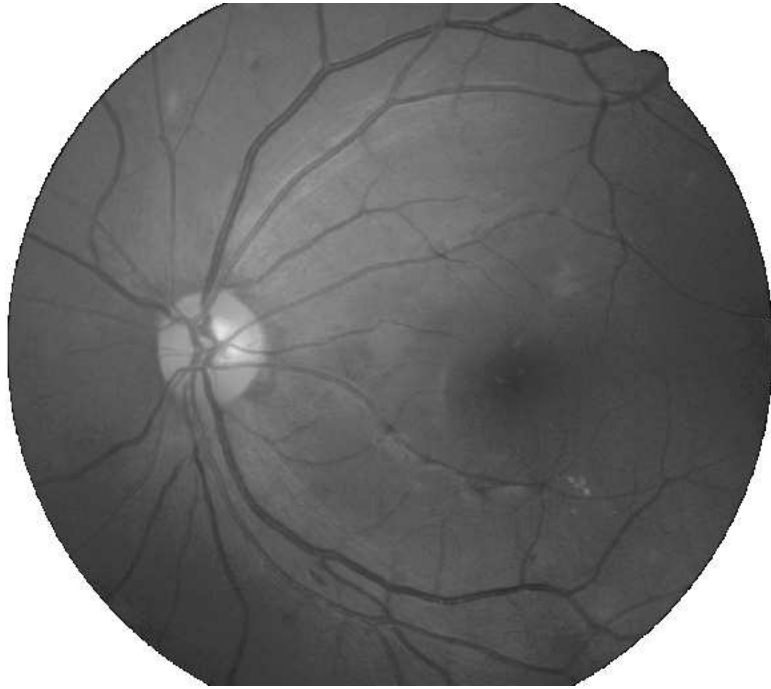
4.1.2 Local Contrast Enhancement

Besides the illuminant difference between two images, the illuminant conditions of one image is also not homogenous. The center part near the optic disc of a retinal image is usually brighter than the boundary due to the ball-shape of the retina and the different light reflection. Local contrast need enhancing in order to localize lesions in the relative dim area of a retinal image. In local enhancement, the image is divided into subimages and the enhancement is done relative to each subimage. In this way, the details over small areas in an image are enhanced.

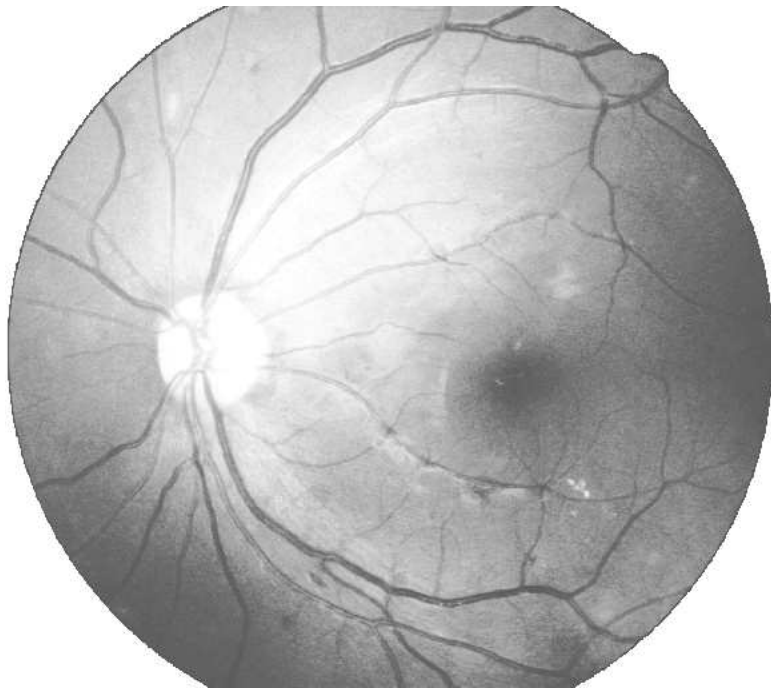
As the low-contrast image's histogram is narrow and centered toward the middle of the gray scale, if we distribute the histogram to a wider range, the quality of the image will be improved. Histogram equalization is similar to histogram specification in section 4.1.1. The color value of a given image are adjusted so that so that the probability density function of color values spread equally. An output image is obtained by mapping each pixel with level t in the input image into a corresponding level w in the output image, where $w \in [0, 1]$. Let $p_r(t)$ and $p_z(w)$ represent the probability density distribution functions of the values of one color channel of the original and desired image, respectively. The histogram of the output image is uniform i.e. $p_z(w) = 1/N$, if there are N possible values for w .

If the equalization is applied to the histogram of a whole image, the result tends to over-expose bright areas and the lesions are not differentiable in the resultant image. Moreover, the dim areas are still relative dim in an image. An example images is shown in Figure 4.8.

In the adaptive histogram equalization, the histogram of color values of one color channel in a $N \times N$ window of an image is generated first, where we set N to be 64. The cumulative distribution of green layer intensities, that is the cumulative



(a) Green Layer



(b) Green Layer after adaptive histogram equalization

Figure 4.8: Histogram Equalization

sum over the histogram, is used to map the input pixel green layer intensities to output green layer intensities.

In order to eliminate artificially induced boundary, input image is divided into 64x64 partially overlapping windows and the neighboring windows are combined to compute the final result. For example, if the first window includes the first 64 columns, then the second window will start from the 33th column. Therefore, each 4 neighboring windows have a common subwindow of size 32x32. In Figure 4.9, the 4 windows are marked out by different texture patterns and they have common subwindow in the center. Since each window has a mapping function computed based on histogram equalization of each window, there are four output values for center subwindow corresponding to the four mapping functions. For each pixel in the center subwindow, its final output value is computed as the average of the four output values.

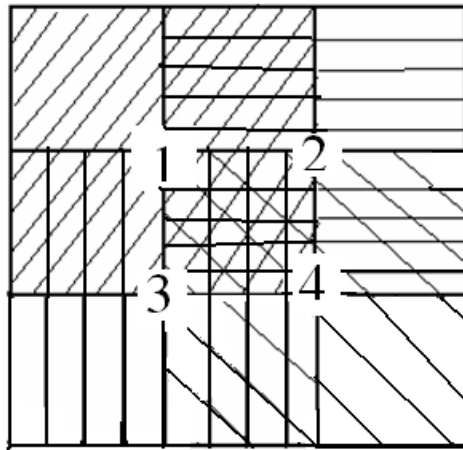


Figure 4.9: Divide Image into 64x64 partially overlapping windows

If the size of the input image is $M \times N$, the algorithm is as follows:

1. Divide each image into windows of size 64x64

$$\text{NumRows} = M/64;$$

NumCols=N/64.

2. Process each window using histogram equalization
 - a) extract a 64x64 window
 - b) make a histogram for this window using 256 bins
 - c) create a mapping for this window using histogram equalization technique
3. Interpolate green layer mappings in order to assemble final image

For each window

Extract four neighboring mapping functions

For each pixel in the window

Apply four mappings to that pixel

Compute the average to obtain the output pixel.

The contrast enhanced version of the image in Figure 4.8 is show in Figure 4.10.

4.2 Candidate Identification Step

After the color normalization and local contrast enhancement, the suspected regions are localized based on the difference map of intensity. The Fuzzy-C means clustering is employed to refine the segmentation of the bright region.

In order to segment potential cotton wool spots, we adopt a coarse segmentation based on intensity difference map of retinal images. The coarse segmentation identifies the high intensity regions by applying a threshold to the difference map. After that, we apply fuzzy c-mean clustering to each identified region to find the proper boundaries of each potential cotton wool spots.

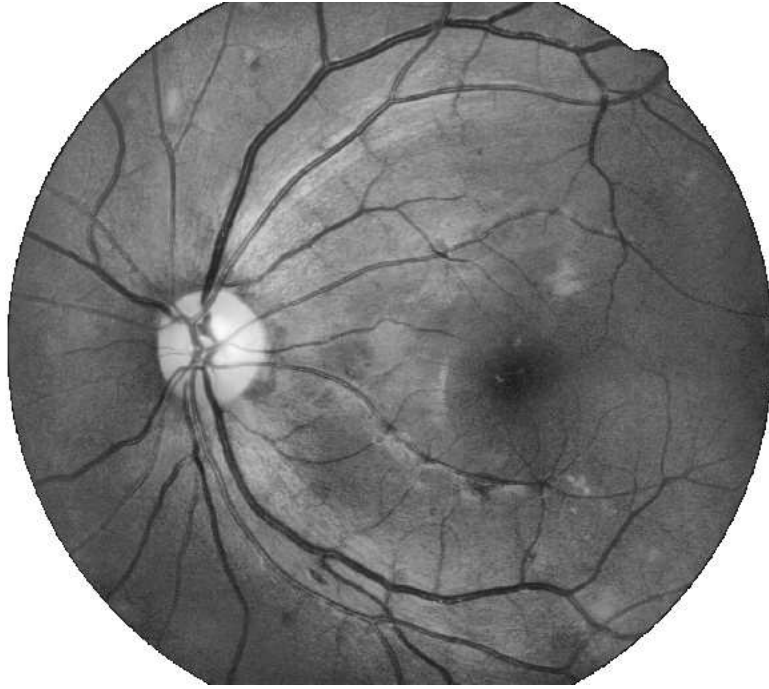


Figure 4.10: Adaptive Histogram Equalization

Recently, many image segmentation algorithms have been proposed according to region edge, and color information. Generally, the color information appeared in the image provides an important feature for human to cluster the desired objects. Based on color information, many techniques including region growing, fuzzy C-means (FCM) and neural network, have been proposed. Region growing is a technique for extracting an image region that is connected based on some predefined criteria. These criteria can be based on color information. Clustering analysis is a statistical classification technique for discovering whether the individuals of a population fall into different groups by making quantitative comparisons of multiple characteristics. Here, Fuzzy C-mean Clustering is used with 3 coordinates in Lab color space to refine the segmentation after localization on difference map.

Fuzzy C-mean Clustering is a clustering method, with which an object has

different membership values for each class. The membership value is the probability of the object belonging to a certain class. Now it has received increasingly attention in image segmentation for its robustness and easy implementation.

The basic idea of the fuzzy clustering method is that patterns are allowed to belong to all clusters with different degrees of membership.

Fuzzy C-means is to find a solution for parameters y_{ji} ($i = 1, \dots, n; j = 1, \dots, g$) for which

$$J = \sum_{i=1}^n \sum_{j=1}^g y_{ji}^r |x_i - m_j|^2 \quad (4.1)$$

is minimized subject to the constraints

$$\sum_{j=1}^g y_{ji} |x_i - m_j|^2 \quad (4.2)$$

In the above formula, x_i is the feature data to be clustered; m_j is the center of each cluster; y_{ij} is the fuzzy partition corresponding to the feature data; n describes the number of the feature data; g is the number of the clusters; and r is the exponent used to adjust the fuzzy degree. Generally, r should be greater than 1, and when r is tend to infinity, the fuzzy degree is increasing. This cost function is used as a control on the updating. That is, we get final result y_{ij} and stop the updating by minimizing the cost function. Moreover, the y_{ij} has the range from 0 to 1 is the main difference with hard c-means which can only have value 0 or 1.

The basic algorithm [1] is iterative and can be stated as follows.

1. Select r ($1 < r < \infty$); initialize the membership function values $y_{ji}, i = 1, \dots, n; j = 1, \dots, g$.

2. E-step: Compute the cluster centers m_j , $j = 1, \dots, g$.

$$m_j = \frac{\sum_{s=1}^n y_{ji}^r x_i}{\sum_{s=1}^n y_{ji}^r} \quad (4.3)$$

3. M-step: Compute the membership function.

$$y_{ij} = \frac{1}{\sum_{s=1}^g \left(\frac{|x_i - m_j|}{|x_i - m_s|} \right)^{\frac{2}{r-1}}} \quad (4.4)$$

4. If not converged, go to step 2.

E-Step is used to obtain the new center of each cluster and M-Step is used to update the fuzzy partition. By repeating E-step and M-step, cluster center m_j and fuzzy partition y_{ji} are updated, until the cost function reaches the minimal value, or can't be reduced anymore, we can get the final cluster information.

When the cluster centers converge, the algorithm stops, i.e.:

$$\sum_{j=1}^g |m_j(k) - m_j(k)|^2 < \varepsilon$$

where ε is a positive value.

In order to reduce the influence of noises, we tried using filtering and wavelet denoising technique to remove noises. Our experiment shows that wavelet denoising technique works better than filtering using 3x3 mean filter. Therefore, the enhanced green layer of retinal image is first de-noised by using 4-level harr wavelet transformation. Then the background is estimated by filtering the smoothed image with a median filter of size 30x30. The difference of the smoothed image and the estimated background is shown in Figure 4.11(d), in which we can see that the bright patches are enhanced.

The result of thresholding difference map is shown in Figure 4.13, where optic disc area detected by Pallawala et al. [26] is removed. It is firstly processed by connected-component labeling. After connected component labeling, each candidate region is given an unique label.

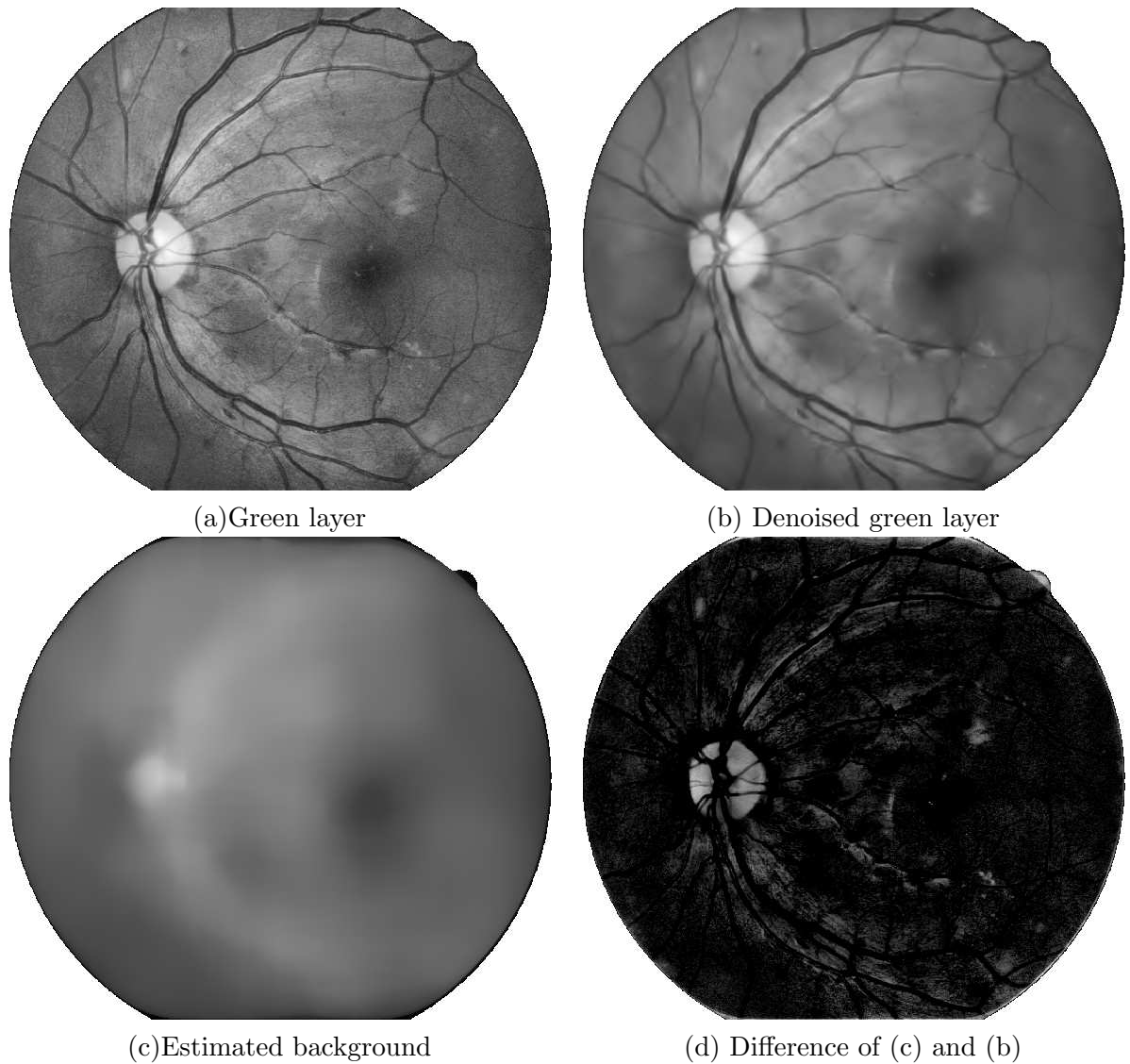


Figure 4.11: Intermediate images

An enclosing window centered at the center of the region is imposed and the window size is either $(x_{max} - x_{min}) \times (y_{max} - y_{min})$, or 32×32 if $(x_{max} - x_{min}) \times$

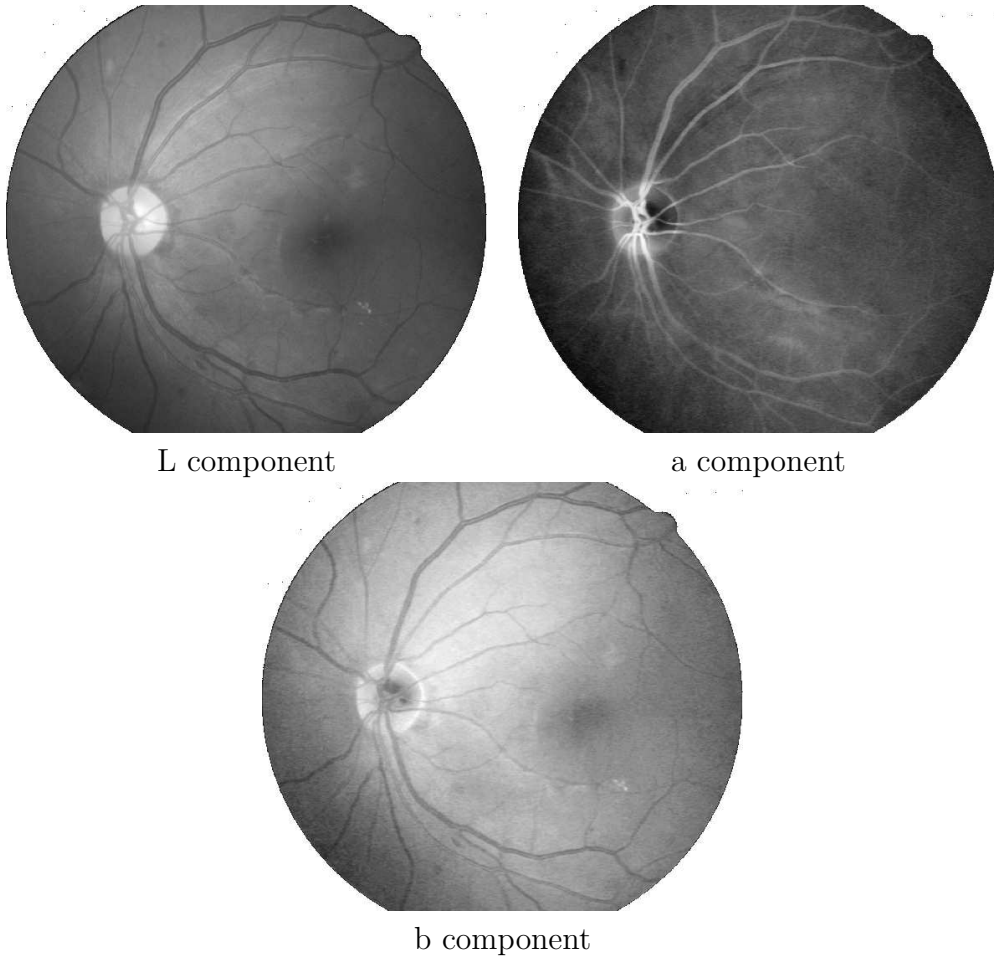


Figure 4.12: Lab Components of image in Fig 4.6

$(y_{max} - y_{min})$ is smaller than 32×32 , where x_{min} is minimum X-coordinate, x_{max} is the maximum X-coordinate, y_{min} is the minimum Y-coordinate and y_{max} is the maximum Y-coordinate of the region. For each window, we used fuzzy clustering to further separate the pixels inside the window into three classes, for most cases, background, vessel, and bright object.

Figure 4.13 shows the candidate regions for a retinal image and on its right, clustering results of four candidate regions are also shown, in which blue areas are bright objects, red areas are vessels or dark objects, and green areas are background.

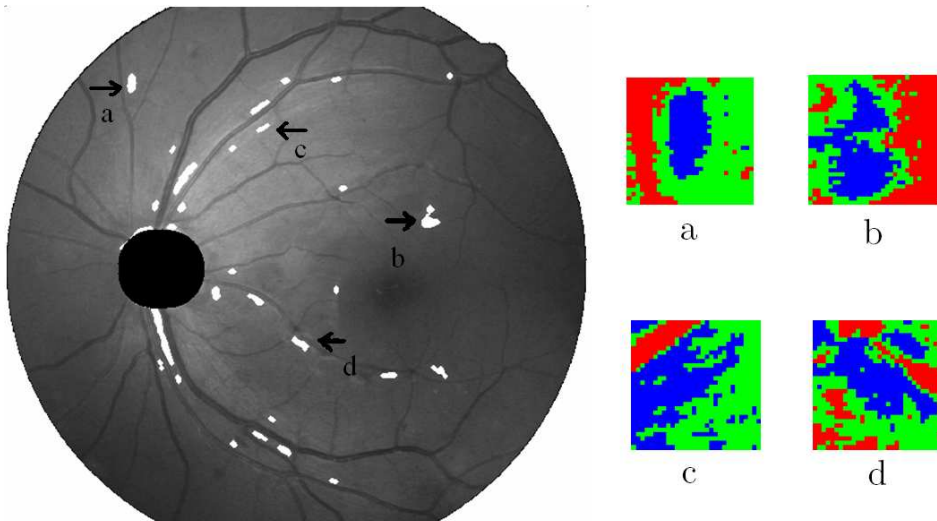


Figure 4.13: Segmentation Fuzzy C-mean clustering

4.3 Validation Step

The candidate identification step finds all the potential cotton wool spots, which contains a lot of noises, reflection along the vessels, etc. The aim of the validation step is to find the true cotton wool spots from all the given candidate regions.

To validate the candidate regions found by coarse-to-fine segmentation, we tried two approaches, SVM classification and eigenimages.

4.3.1 Eigenimages

In this section, we examine how eigenimages can be used to validate cotton wool spots.

Eigenvectors x of a n -by- n matrix A are defined as the length n column vectors for which the following equation holds: $Ax = \lambda x$, with λ being the corresponding eigenvalue. These eigenvectors are particularly useful in the Karhunen-Loève Transform (KLT, also called Hotelling Transform or Principal Component Analysis PCA). PCA based approach has been widely applied in face recognition [19,33], texture classification and retrieval [8]. In medical imaging area, some research has shown the application of PCA analysis in optic disc localization [21].

The problem of cotton wool spot detection is similar to face recognition since cotton wool spots have some texture pattern. The idea of template matching using PCA is to perform cross-covariances with the given image and a template that is representative of the image. Therefore, in application to cotton wool spots detection, the template should be a representative cotton wool spot - being either an average image of all the cotton wool spots in the training images. In our case, the first step was to crop out the cotton wool spots from retinal images and these cotton wool spot images as our set of training images. In our case, 20 cotton wool spots in 15 different images were cropped out manually. After the images were acquired, they were resized to the average size, 20×14 pixels. Their intensity is adjusted linearly to the same range so that the illumination difference is eliminated. They are considered as a column vector of size $N = m \times n$. N is set to 20×14 in our case. Let Γ_i be the vector of a image $i = 1 \dots K$, obtained by

row-scanning the two dimensional images with $N = m \times n$ pixels in each images. The average image vector is computed as

$$\Psi = \frac{1}{K} \sum_{i=1}^K \Gamma_i$$

Samples of training images and their average images are shown in Figure 4.14. Let $\Phi_i = \Gamma_i - \Psi$ denotes the difference between the training image and the average

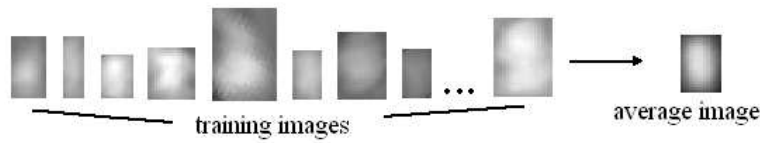


Figure 4.14: Training images and average image

image. Then the covariance matrix C can be obtained by:

$$C = \frac{1}{K} \sum_{i=1}^K \Phi_i \Phi_i^T = \frac{1}{K} G G^T, \text{ where } G = [\Phi_1 \Phi_2 \dots \Phi_K].$$

A set of eigenvalues λ_i and eigenvectors v_i can be computed for $G^T G$. Thus we have: $G^T G v_i = \lambda_i v_i$ where v_i are the eigenvectors, and λ_i are the corresponding eigenvalues. From this result, it is evident that multiplying this equation by G will give us the eigenmatrices of $C = G G^T$, as $G G^T G v_i = \lambda_i G v_i$. Therefore, $G v_i$ is eigenvector of C . Based on v_i , we computed the eigenvector u_i for C . u_i is a linear combination of the original training image vectors and arranged in descending order according to its corresponding eigenvalue. The vectors u_i are actually images, called eigenimages.

The first K' eigenvectors $u_i, i = 1, \dots, K'$ are regarded dominant. Detection using eigenimages is to test whether or not a candidate patch was a cotton wool spot. This method is based on the assumption that the space of cotton wool spots can be spanned by the set of eigenvectors $u_i, i = 1, \dots, K'$. To test a candi-

date patch, the patch is firstly cropped out by its bounding rectangle. Then this rectangle image Γ is resized to the same size as the average image. Its intensity is linearly adjusted to the same range. To project the image to the space of cotton wool spots, the mean image Ψ is subtracted first: $\Phi = \Gamma - \Psi$. The image Γ is reconstructed by the following transformation:

$$w_i = u_i \cdot (\Gamma - \Psi), i = 1, 2, \dots, K.$$

w_i denotes the contribution of Φ_i in representing the input image Γ . Let Φ_p denote the projection of Φ , where $\Phi = \Gamma - \Psi$. The input image can be reconstructed as Γ_p :

$$\Gamma_p = \Psi + \Phi_p = \Psi + \sum_{i=1}^{K'} w_i u_i$$

To measure the likeness of a input candidate to be cotton wool spot, the distance between the original image and its projection is calculated. Their Euclidean distance E is computed as:

$$\begin{aligned} E &= \|\Phi - \Phi_p\| \\ &= (\Phi - \Phi_p)^T (\Phi - \Phi_p) \\ &= (\Phi^T \Phi - \Phi_p \Phi_p^T - (\Phi - \Phi_p)^T \Phi_p - \Phi_p^T (\Phi - \Phi_p)) \end{aligned}$$

Since Φ_p is the projection of Φ , Φ_p is orthogonal to $\Phi - \Phi_p$. Therefore, $(\Phi - \Phi_p)^T \Phi_p$ and $\Phi_p^T (\Phi - \Phi_p)$ are equal to zero. Since $\Phi_p = \sum_{i=1}^{K'} w_i^2$, the computation of E can be simplified as $E = \Phi^T \Phi - \sum_{i=1}^{K'} w_i^2$.

Since cotton wool spots appear in retinal images in different rotations, we rotate a candidate patch by 0, 45, 90, 135 degrees, and take the shortest the Euclidean distance of the four, which is corresponding to the best match. The Euclidean distance measures the similarity between the input image to the training cotton wool spot images. A large Euclidean distance implies the candidate

region is unlikely cotton wool spots. The Euclidean distances between reconstructed images of the training images to the training images are computed. The mean distances (denoted by m) and their standard deviation (denoted by std) are used to compute a threshold. The threshold is defined as $m + 5 * std$. A input image with Euclidean distance larger than the threshold is considered as non-cotton wool spots.

4.3.2 SVM Classification

After Fuzzy C-means clustering, for each local window, we have three clusters, background, vessel and bright regions. We need to classify these segmented bright regions into true cotton wool spots and non-cotton wool spots (noises, reflection along the vessel). In this section, we investigate the Support Vector Machine's application to this task of classifying the segmented bright regions.

Support Vector Machines have become an increasingly popular tool for machine learning tasks. They have been successfully applied to various pattern recognition and medical imaging problems. The reason of using SVM is the fact that SVM is very well grounded from the mathematical point of view [31].

When used for classification, the SVM algorithm creates a hyperplane that separates the data into two classes with the maximum-margin. Given training examples labeled either "+1" or "-1", a maximum-margin hyperplane is identified which splits the "+1" from the "-1" training examples, such that the distance between the hyperplane and the closest examples (the margin) is maximized.

In order to classify cotton wool spots from the non-cotton wool spots, we need to select those features which differentiate cotton wool spots from non-cotton wool spots. After the clustering, the cotton wool spots usually lie in the center of the local window. Their shapes are usually more compact than noises. On the other

hand, the reflection areas along the vessels are usually elongated. From these analysis, we have selected the following features:

1. Lab Components

The 3 values for Lab Components.

2. Elongation

Eigenaxes are defined by eigenvalues.

Suppose

$$E = \begin{bmatrix} x_1 & y_1 \\ x_2 & y_2 \\ \cdots & \cdots \\ x_N & y_N \end{bmatrix}$$

, where x_i and y_i are the x-coordinate and y-coordinate of i-th point on the edge. Suppose the covariance of E is C and V_1 and V_2 is two eigenvectors of C, where V_1 is associated with larger eigenvalue r_1 and V_2 is associated with smaller eigenvalue r_2 . Then V_1 and V_2 is the major and minor axis of the shape, while r_1 and r_2 are proportional to the length of the major axis and minor axis. Thus elongation = r_1/r_2 ;

3. *Compactness = Perimeter²/Area*

Perimeter is defined by the length of the edge of a region. The distance between two diagonal points are estimated as $\sqrt{2}$.

Suppose there are N points lying on the edge and E_i is a point lying on the edge, $i=1\dots N$. Then the perimeter is computed as follows:

For $n = 1 : N$

$$U_n = E_n.x + E_n.y * i$$

$$Perimeter = \sum_{n=1}^N |U_n - U_{n-1}|$$

Area is defined as the total number of pixels inside the region.

4. Distance between centroid to window center

Centroid is the center of mass (color intensity in this case). Suppose $centroid_x$ and $centroid_y$ are x-coordinate and y-coordinate of centroid, $color(x, y)$ is the intensity value at pixel (x, y) . The following algorithm computes the two coordinates.

Region-Based Centroid Estimation

$centroid_x = 0$; $centroid_y = 0$;

totalWeight=0;

For x=1 to LengthX do

 For y=1 to LengthY do

 If (q(x,y)==1)

$centroid_x = centroid_x + x \times color(x, y)$;

$centroid_y = centroid_y + y \times color(x, y)$;

 totalWeight = totalWeight+color(x,y);

 end

 end

end

$centroid_x = centroid_x / totalWeight$;

$centroid_y = centroid_y / totalWeight$;

After computing centroid, the distance from window center to centroid is computed as $\sqrt{(Xcenter - centroid_x)^2 + (Ycenter - centroid_y)^2}$, where $Xcenter$ is x-coordinate and $Ycenter$ is y-coordinate of window center.

5. Number of Pixels near the center

For each local window, we define a smaller window centered at the same center of the original window and its size is half of the original window(Figure 4.15). The total number of pixels of a candidate region that lie in the smaller window is counted as this feature.

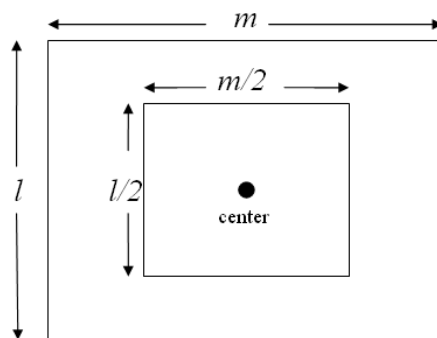


Figure 4.15: Smaller center window

6. Number of pixels at the boundary of the rectangular window

If the red area grows until the boundary, it is less probable that the red area is CWS. This feature is defined as the number of pixels that lie in the first column, last column, first row, last row of the window (the gray color in Figure 4.16).

7. Number of pixels next to vessels

When a blue area's elongation is larger than certain value, it is probably the vessel. If the red area is quite near the blue area and the direction of the edges are similar, then the red area is not CWS but the reflection along the vessels.

Firstly both areas are dilated using morphological operation by element structure with disk of radius 1. After this dilation, the overlapping pixels

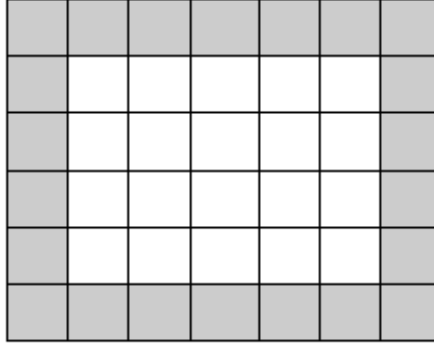


Figure 4.16: Boundary of a window

correspond to the neighboring pixels of two areas. Thus, the overlapping pixels are counted and its total number is taken as this feature.

In our work, we used SVM library package developed by C. C. Chang et al. [2]. The radial basis function $\exp(-\gamma * |u - v|^2)$, where $\gamma = 1/k$ and k is the number of features, is used as the function. For each candidate region (red area after fuzzy clustering), those features described in above are computed and input into the SVM classifier. The regions from 64 images that graded by retinal specialists are prepared as training data. There more negative examples than positive examples. To make the training set balanced, we randomly selected the same number of negative examples and combined with all the positive examples as a training set. The trained model is tested on more than 1000 images. The experiment results will be shown in next section.

4.4 Experiment

We use the same real world dataset of 1198 consecutive images to evaluate the cotton wool spots detection algorithm. These images are graded by two retinal

specialists. Out of the 1198 images, a total of 260 regions have been marked as cotton wool spots by the two retinal specialists. They agree on 221 regions and disagree on 39 regions. Table 4.1 compares the number of regions detected by our algorithms with the number of the regions identified by the two retinal specialists. We denote the set of cotton wool spots identified by Retinal specialist 1 as R1 and the set of cotton wool spots identified by Retinal specialist 2 as R2. The first column shows the number of cotton wool spots detected by our two algorithms, which are also identified by both retinal specialists. The second column shows the number of cotton wool spots detected by our algorithms, which are identified by at least one of the retinal specialists. The third column shows the number of cotton wool spots detected by our algorithms, which are not identified by any retinal specialist.

	$R1 \cap R2$	$R1 \cup R2$	$\notin (R1 \cup R2)$
R1	221	240	0
R2	221	241	0
Candidate regions	221	231	31089
Eigenimages	106	110	337
SVM Classification	187	211	795

Table 4.1: Comparison of the number of regions identified

Due to the weak characteristics of cotton wool spots, our systems detected some false cotton wool spots. The cotton wool spots sometimes are hard to differentiate from other lesions like drusen. In Figure 4.4, the two false cotton wool spots identified by SVM classification are shown.

The 260 regions marked by the two retinal specialists are contained in 73 images. We say an image contains cotton wool spots if it contains at least one cotton wool spot. Out of the 1198 images, the two specialists agree that 71 images contain cotton wool spots and 1125 images do not contain cotton wool

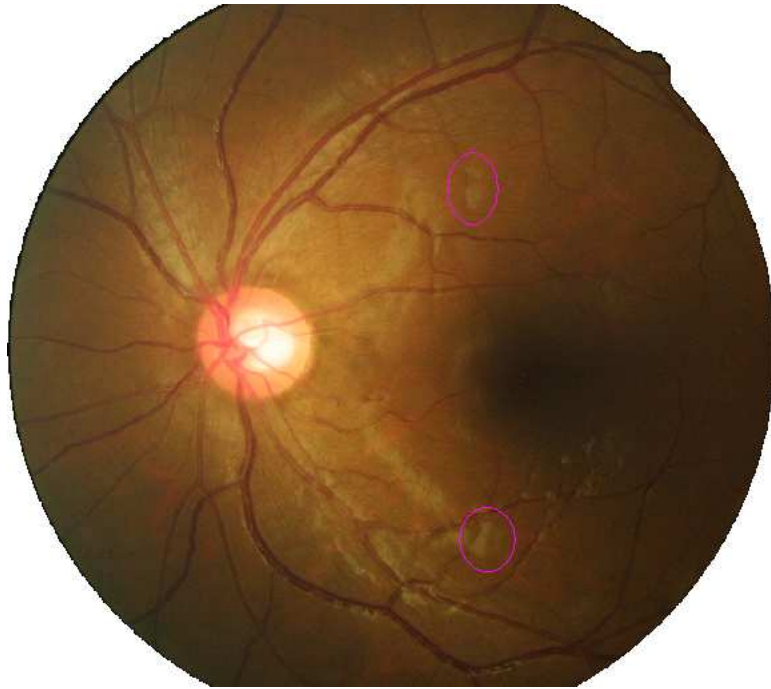


Figure 4.17: False cotton wool spots detected by SVM classification

spots. They disagree on 2 images. Our eigenimage approach is able to detect the cotton wool spots in 44 images out of the 71 images they agreed on and our SVM approach finds cotton wool spots in all 71 images.

In table 4.2, the images in which our algorithms detected cotton wool spots are compared with the images in which the two retinal specialists found cotton wool spots. We denote the set of images in which Retinal specialist 1 found cotton wool spots as I_1 and the set of images in which Retinal specialist 2 found cotton wool spots as I_2 . The first column shows the number of images detected by our two algorithms, which are also identified by both retinal specialists. The second column shows the number of images detected by our algorithms, which are identified by at least one of the retinal specialists. The third column shows the number of images detected by our algorithms, which are not identified by any retinal specialist.

	$I1 \cap I2$	$I1 \cup I2$	$\notin (I1 \cup I2)$
I1	71	1	0
I2	71	1	0
Eigenimages	44	1	245
SVM Classification	71	2	193

Table 4.2: Comparison of the number of images identified

We compute the sensitivity and specificity based on the images the two specialists agree on, i.e. 71 images contain cotton wool spots and 1125 images do not contain cotton wool spots, Table 4.4 shows the sensitivity and specificity of our two approaches. Eigenimage approach can achieve 62.1% sensitivity and 78.2% specificity.

Training Set	Sensitivity	Specificity
1	100%	83.9%
2	100%	81.5%
3	100%	83.0%
Average	100%	82.8%

Table 4.3: SVM Classification Result

Approaches	Sensitivity	Specificity
Eigenimages	62.1%	78.2%
SVM Classification	100%	82.8%

Table 4.4: Experiment Results of the Two Approaches

For SVM classification, only the regions the two specialists agree on are used as training data. 32 images are selected from 71 images in which the two specialists found cotton wool spots and another 32 images from the 1125 images in which the two specialists do not found any cotton wool spots. There are 3266 segmented bright regions in these 64 images, and among them there are only 57 cotton wool spot regions. We randomly selected 57 non-cotton-wool-spot regions from them and input them together with 57 cotton wool spots to SVM classifier for training.

The rest of the images are used as testing images. Since the negative examples are chosen randomly, the experiment is conducted 3 times. That is we have 3 different models trained with 3 different training dataset. The testing results for these three models are shown in Table 4.3. On average, the classification approach can achieve 100% sensitivity and 82.8% specificity on image level.

The experiment results of these two approaches summarized in Table 4.4 show that the SVM classification has the better performance. The basic idea of Eigenimage approach is template matching. Given that the cotton wool spots do not have uniform shape, the Eigenimage approach does not perform as well as SVM classification approach.

Chapter 5

Conclusion and Future work

In this research, we have developed algorithms on the detection of bright lesions such as hard exudates and cotton wool spots in retinal images. The proposed wavelet-based algorithm to detect hard exudate has sensitivity of 97.9% and specificity of 78.2%. To our best of knowledge, no work has been done using wavelet to detect hard exudates. Our algorithm were evaluated using 1198 retinal images collected from clinics.

Existing work were focused on detecting lesions and do not identify cotton wool spots directly. We described how eigenimages and SVM classification can be utilized to detect cotton wool spots. We also demonstrate the robustness and reliability of our methods by evaluating on a realworld dataset of 1198 images. Eigenimage approach can achieve 62.1% sensitivity and 78.2% specificity and the classification approach can achieve 100% sensitivity and 82.8% specificity on image level.

Future work would be focused on developing algorithms to detect other types of lesions, such as microaneurysms and hemorrhages. These are dark lesions in retinal images. Similar to hard exudates, the size of microaneurysms is relatively

small. The wavelet application can be investigated to detect microaneurysms and hemorrhages. We can also investigate the application of Fuzzy C-Means clustering and SVM classification in detecting microaneurysms and hemorrhages.

Bibliography

- [1] J. C. Bezdek, Pattern Recognition with Fuzzy Objective Function Algorithms, Plenum Press, New York, 1981.
- [2] C. C. Chang and C. J. Lin, LIBSVM : a library for support vector machines, 2001. Software available at <http://www.csie.ntu.edu.tw/~cjlin/libsvm>.
- [3] I. Daubechies, Ten lectures on wavelets, SIAM, 1992.
- [4] Early Treatment Diabetic Retinopathy Study Research Group. Fundus Photographic Risk Factors for Progression of Diabetic Retinopathy. ETDRS Report No. 12, in Ophthalmology, Vol. 98, pp. 823-833, 1991.
- [5] B. M. Ege, O. K. Hejlesen, O. V. Larsen, K. Møller, B. Jennings, D. Kerr, D.A. Cavan, Screening for Diabetic Retinopathy Using Computer Based Image Analysis and Statistical Classification, *Computer Methods and Programs in Biomedicine*, Vol. 62, pp. 165-175, 2000.
- [6] B. Fang, W. Hsu, M. L. Lee, Reconstruction of vascular structures in retinal images, in *Proceedings. ICIP2003, Barcelona, Spain*, Vol. 2, pp. 157-160, 2003.
- [7] R. C. Gonzalez and R. E. Woods, Digital Image Processing, Prentice-Hall, 2002

- [8] M. J. Gangeh, M. Bister, M. Hammandlu, Multiresolution eigenimages for texture classification, *Proceeding of International Conference on Acoustics, Speech, and Signal Processing*, Vol. 5, pp. 829-32, 2004.
- [9] G. G. Gardner, D. Keating, T. H. Williamson, A. T. Elliott, Automatic Detection of Diabetic Retinopathy Using an Artificial Neural Network: A Screening Tool, *The British Journal of Ophthalmology*, Vol. 80(11), pp. 940-944, 1996.
- [10] M. H. Goldbaum, N. P. Katz, M. Nelson, The Discrimination of Similarly Colored Objects in Computer Images of the Ocular Fundus, *Investigative Ophthalmology and Visual Sciences*, Vol. 31, pp. 617-623, 1990.
- [11] R. C. Gonzalez and R. E. Woods, *Digital Image Processing*, Prentice-Hall, 2002
- [12] A. M. P. Hamilton, M. W. Ulbig, P. Polkinghorne, *Management of Diabetic Retinopathy*, BMJ Publishing Group, 1996.
- [13] T. Hellstedt and I. Immonen, Disappearance and Formation Rates of Microaneurysms in Early Diabetic Retinopathy, *British Journal of Ophthalmology*, Vol. 80, pp. 135-139, 1996.
- [14] W. Hsu, P. M. D. S. Pallawala, M. L. Lee, K.G. Au Eong, The Role of Domain Knowledge in the Detection of Retinal Hard Exudates, *Proceedings of IEEE Conference on Computer Vision and Pattern Recognition*, Vol. 2, pp. 246-251, 2001.
- [15] N. Katz, M. Goldbaum, M. Nelson, S. Chaudhuri, An Image Processing System for Automatic Retina Diagnosis, *Three-Dimensional Imaging and Remote Sensing Imaging*, SPIE, Vol. 902, pp. 131-137, 1988.

- [16] A. Laine, Wavelets in Temporal and Spatial Processing of Biomedical Images, *Annual Review in Biomedical Engineering*, vol. 2, pp. 511-550, 2000.
- [17] A. F. Laine, S. Schuler, F. Jian, and W. Huda, Mammographic feature enhancement by multiscale analysis, *IEEE Trans. Med. Imag.*, vol. 13, pp. 725-740, Feb. 1992.
- [18] S. C. Lee, E. T. Lee, R. M. Kingsley, Y. Wang, D. Russell, R. Klein, Ann Warn Comparison of Diagnosis of Early Retinal Lesions of Diabetic Retinopathy Between a Computer System and Human Experts *Arch Ophthalmol*, vol.119, pp.509 - 515, Apr 2001.
- [19] S. J. Lee, S. B. Jung, J. W. Kwon, S. H. Hong, Face detection and recognition using PCA, TENCON 99. Proceedings of the IEEE Region 10 Conference, vol.1, pp.84-87.
- [20] L. Leistritz, D. Schweitzer, Automated Detection and Quantification of Exudates in Retinal Images, *SPIE: Applications in digital Image Processing*, Vol. 2298, pp. 690-696, 1994.
- [21] H. Li, O. Chutatape, Automatic Location of Optic Disc in Retinal Images, *Proceedings of International Conference on Image Processing*, pp. 837-840, 2001.
- [22] H. Li, O. Chutatape, Automated Feature Extraction in Color Retinal Images by a Model Based Approach, *IEEE Transactions on Biomedical Engineering*, vol. 51, no. 2, pp. 246-254, 2004.
- [23] H. Li, O. Chutatape, S. M. Krishnan, D. Wong, Automatic Detection of Exudates in the Fundus Image, *Proceedings of Image and Vision Computing New Zealand*, pp. 322-326, 2000.

- [24] Z. Liu, C. Opas, S. M. Krishnan, “Automatic Image Analysis of Fundus Photograph”, in *Proceedings of IEEE International Conference on Engineering in Medicine and Biology*, Vol. 2, 524-525, 1997.
- [25] A. Osareh, M. Mirmehdi, B. Thomas, R. Markham, Comparative Exudate Classification using Support Vector Machines and Neural Networks, *5th International Conference on Medical Image Computing and Computer-Assisted Intervention*, pp. 413–420, 2002.
- [26] P. M. D. S. Pallawala, Wynne Hsu, M. L. Lee, K. G. Au Eong: Automated Optic Disc Localization and Contour Detection Using Ellipse Fitting and Wavelet Transform. *ECCV (2) 2004*: 139-151
- [27] R. P. Phillips, T. Spencer, P. G. B. Ross, P. F. Sharp, J.V. Forrester, Quantification of Diabetic Maculopathy by Digital Imaging of the Fundus, *Eye*, vol. 5, pp. 130-137, 1991.
- [28] R. Phillips, J. Forrester, P. Sharp, Automated Detection and Quantification of Retinal Exudates, *Graefe’s Archive for Clinical & Experimental Ophthalmology*, vol. 231, pp. 90-94, 1993.
- [29] C. Sinthanayothin, J. F. Boyce, T. H. Williamson, H. L. Cook, E. Mensah, S. Lal et al. Automated detection of diabetic retinopathy on digital fundus images. *Diabet Med*, vol. 19, pp. 105-112, 2002.
- [30] R. T. Smith, Takayuki Nagasaki, J. R. Sparrow, I. Barbazettp, C. CW. Klaver and J. K. Chan, A Method of Drusen Measurement Based on the Geometry of Fundus Reflectance, *BioMedical Online*, vol.2, 2003
- [31] A.J. Smola, Bernhard Scholkopf, A Tutorial on Support Vector Regression, 1998

- [32] R. N. Strickland, Wavelet transform for detecting microcalcifications in mammograms, *IEEE Trans. Med. Imaging*, vol. 15, pp. 218-229, 1996.
- [33] M. A. Turk and A. P. Pentland, Eigenfaces for recognition, *Journal of Cognitive Neuroscience*, vol. 3, pp. 71 - 86, 1991
- [34] M. Unser, A. Aldroubi, A Review of Wavelets in Biomedical Applications, *Proceedings of the IEEE*, vol. 84, no. 4, pp. 626-638, 1996.
- [35] D. Unser, M. Dumskyj, M. Himaga, T. H. Williamson, S. Nussey and J. Boyce, Automated Detection of Diabetic Retinopathy in Digital Retinal Images: a Tool of Diabetic Retinopathy Screening, *Diabetes UK. Diabetic Medicine*, vol. 21, pp. 84-90, 2003.
- [36] H. Wang, W. Hsu, K. G. Goh, M. L. Lee, An Effective Approach to Detect Lesions in Color Retinal Images, *IEEE Conference on Computer Vision and Pattern Recognition*, pp. 2181-2186, 2000.
- [37] N. P. Ward , S. Tomlinson, C. J. Taylor, Image Analysis of Fundus Photographs, *Ophthalmology*, Vol. 96(1), pp. 80-86, 1989.
- [38] J. B. Weaver, X. Yansun, D. M. Jr. Healy, and L. D. Cromwell, Filtering noise from images with wavelet transforms, *Magnetic Resonance in Medicine*, vol.24, pp. 288-295, 1991.
- [39] World Health Organization Fact Sheet No. 138, World Health Organization, Revised April 2002.
- [40] V. Vapnik, *Statistical Learning Theory*, Springer-Verlag, New York, 1995.

- [41] X. Zhang, O. Chutatape, Detection and Classification of Bright Lesions in Color Fundus Images, *IEEE International Conference on Image Processing*, Vol. 1, pp. 139 - 142, 2004.